

# Geochemistry, Geophysics, Geosystems

## RESEARCH ARTICLE

10.1029/2019GC008786

### Key Points:

- IODP Expedition 316 drilling across two fault zones in the Nankai accretionary prism allowed the recovery of intact cores of fault rocks
- Fault rocks consist of microbreccia and weakly foliated gouge along sharp planar fault surfaces and foliated clayey gouge in millimeter-thick shear zones
- Microbreccia and weakly foliated gouge suggest propagation of seismic slip along fault surfaces, while foliated gouge suggests aseismic or slow slip along shear zones

### Supporting Information:

- Supporting Information S1

### Correspondence to:

O. Fabbri,  
olivier.fabbri@univ-fcomte.fr

### Citation:

Fabbri, O., Goldsby, D. L., Chester, F., Karpoff, A. M., Morvan, G., Ujiie, K., et al. (2020). Deformation structures from splay and décollement faults in the Nankai accretionary prism, SW Japan (IODP NanTroSEIZE Expedition 316): Evidence for slow and rapid slip in fault rocks. *Geochemistry, Geophysics, Geosystems*, 21, e2019GC008786. <https://doi.org/10.1029/2019GC008786>

Received 31 OCT 2019

Accepted 24 APR 2020

Accepted article online 25 APR 2020

## Deformation Structures From Splay and Décollement Faults in the Nankai Accretionary Prism, SW Japan (IODP NanTroSEIZE Expedition 316): Evidence for Slow and Rapid Slip in Fault Rocks

O. Fabbri<sup>1</sup> , D. L. Goldsby<sup>2</sup> , F. Chester<sup>3</sup>, A. M. Karpoff<sup>4</sup>, G. Morvan<sup>5</sup>, K. Ujiie<sup>6</sup>, A. Yamaguchi<sup>7</sup> , A. Sakaguchi<sup>8</sup>, C. F. Li<sup>9</sup> , G. Kimura<sup>10</sup> , A. Tsutsumi<sup>11</sup> , E. Screaton<sup>12</sup> , and D. Curewitz<sup>13</sup>

<sup>1</sup>UMR CNRS 6249, Université de Franche-Comté, Besançon, France, <sup>2</sup>Earth and Environmental Sciences, School of Arts and Sciences, University of Pennsylvania, Philadelphia, PA, USA, <sup>3</sup>Center for Tectonophysics, Department of Geology and Geophysics, Texas AandM University, College Station, TX, USA, <sup>4</sup>Institut de Physique du Globe de Strasbourg (IPGS), UMR7516, Université de Strasbourg, Strasbourg, France, <sup>5</sup>Laboratoire d'Hydrologie et de Géochimie de Strasbourg (LHyGeS), UMR7517, Université de Strasbourg, Strasbourg, France, <sup>6</sup>Doctoral Program in Earth Evolution Sciences, Graduate School of Life and Environmental Sciences, University of Tsukuba, Tsukuba, Japan, <sup>7</sup>Department of Ocean Floor Geoscience, Atmosphere and Ocean Research Institute, University of Tokyo, Kashiwa, Japan, <sup>8</sup>Graduate School of Science and Technology for Innovation, Yamaguchi University, Yamaguchi, Japan, <sup>9</sup>Department of Marine Sciences, Zhejiang University, Zhoushan, China, <sup>10</sup>Department of Marine Environment and Resources, Tokyo University of Marine Science and Technology, Tokyo, Japan, <sup>11</sup>Division of Earth and Planetary Sciences, Graduate School of Science, Kyoto University, Kyoto, Japan, <sup>12</sup>Department of Geological Sciences, University of Florida, Gainesville, FL, USA, <sup>13</sup>Department of Earth Sciences, 204 Heroy Geology Laboratory, Syracuse University, Syracuse, NY, USA

**Abstract** Drilling during IODP NanTroSEIZE Expedition 316 led to the recovery of cores from the *basal décollement* in the frontal part of the Nankai accretionary prism and from a *splay fault* branching from the décollement at 25-km landward of the prism toe. The core from the *splay fault* shows a main shear zone and two secondary shear zones. The main shear zone can be divided into two subzones. The upper subzone consists of a 1.2-mm thick foliated gouge zone truncated downward by a through-going fault encompassing a 0.4-mm thick weakly foliated gouge interval. A nearby 200- $\mu$ m thick granular injection vein is interpreted as derived from the fault. The lower subzone consists of a foliated clayey gouge. A 70- $\mu$ m thick granular injection vein is also observed along this subzone. In the *basal décollement* core, microstructures consist of foliated gouge along a flat-lying shear zone and seven flat-lying or gently dipping secondary or incipient shear zones above. A redox front lies beneath the main shear zone. The shear zone and the redox front are truncated by a fault surface outlined by microbreccia developed at the expense of the overlying foliated gouge. Foliated gouge from the shear zones is tentatively interpreted as resulting from slow slip or aseismic creep. The weakly foliated gouge, the microbreccia, and the granular injection veins are interpreted as resulting from coseismic slip. The presence of the redox front beneath the main shear zone of the décollement fault core is interpreted as a consequence of oxidizing fluid flow along the microbreccia-bearing fault.

**Plain Language Summary** To understand why some large subduction zone earthquakes are followed by destructive tsunamis and others are not is a key issue in seismic hazard assessment. Tsunami genesis is suspected to depend mainly on the capacity of faults in shallow parts of subduction zones to either transfer seismic slip from hypocentral depth upward or to dampen it before it reaches the surface. Expedition 316 of the IODP NanTroSEIZE program drilled across and retrieved cores from two major fault zones in the frontal part of the Nankai accretionary prism off Kii Peninsula. The rocks constituting the cored fault zones show microstructures which testify to both slow slip (plate tectonic steady-state creep velocity or slow slip transient event velocity) and rapid slip (conventional earthquake slip velocity). It follows that in the Nankai Trough off Kii Peninsula, earthquake rupture can propagate along either of the major faults known there.

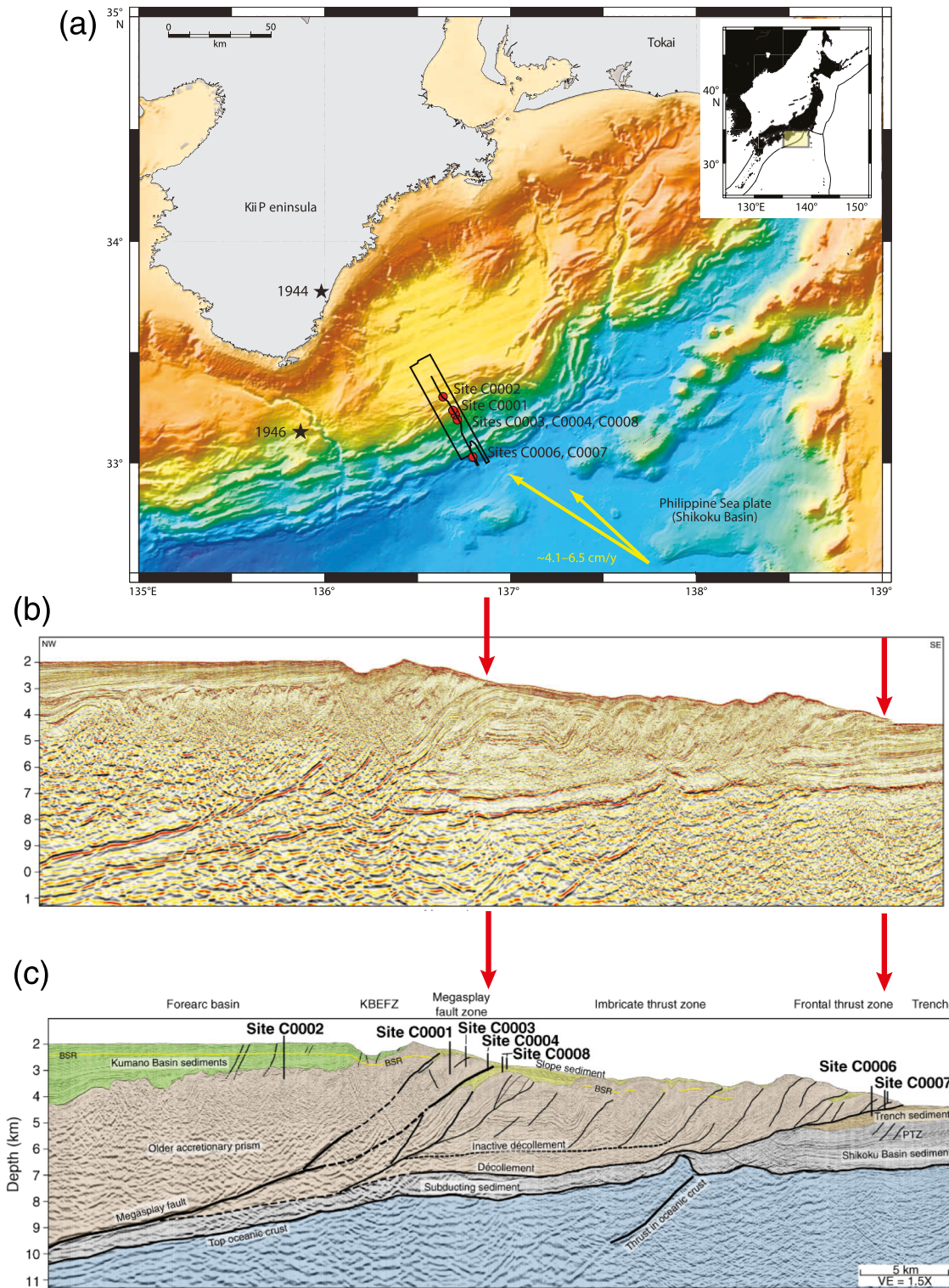


**Figure 1.** (a) Bathymetric map of the Nankai Trough south of the Kii Peninsula showing the location of IODP NanTroSEIZE Stage 1 drilling sites (after Tobin et al., 2009). Relevant to this study are Sites C0004 (splay fault) and C0007 (basal décollement). Stars indicate the epicenters of the 1944  $M_w$  8.1 Tonankai and 1946  $M_w$  8.3 Nankai earthquakes (after Ichinose et al., 2003). Black box = location of the 2006 3-D seismic survey, black line = arbitrary line extracted from 3-D seismic volume (see below, b and c), yellow arrows = computed far-field convergence vectors between Philippine Sea plate and Japan (Heki, 2007; Seno et al., 1993). Inset shows the geodynamical setting of Nankai Trough. (b) Seismic profile along the black line shown in (a). Red arrows point at the location of drilling Sites C0004 and C0007 which are relevant to this study. (c) Same as (b) with interpretative line drawing of major faults and location of IODP NanTroSEIZE drilling sites.

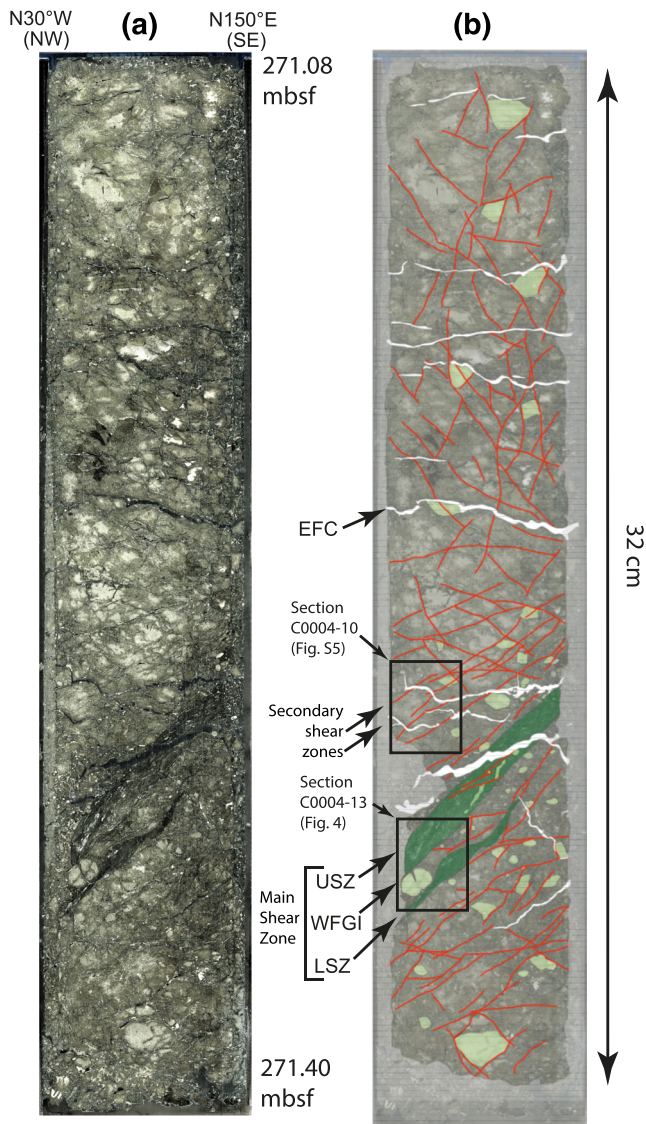


**Figure 2.** (a) Photograph and (b) interpretative sketch of the studied splay fault gouge zone intact core interval (interval 316-C0004D-28R-2, 17–49 cm). The rectangles show the position of the studied polished thin sections C0004–13 (Figure 4) and C0004–10 (Figure S5 in the supporting information). USZ: upper subzone; WFGI: weakly foliated gouge interval; LSZ: lower subzone; EFC: epoxy-filled crack. Red lines are (closed) fractures.

## 1. Introduction

Seismic reflection profiles across active convergent margins show that, in addition to well-recognized basal décollement thrust faults and associated in-sequence frontal thrusts, sedimentary accretionary prisms are crosscut by out-of-sequence thrusts, also called splay or megasplay faults, branching from the plate interface at depth and cutting the accreted sediments up to the sea floor (Arai et al., 2016; Collot et al., 2008; Hsu et al., 2013; Melnick et al., 2012; Moore et al., 1991; Park et al., 2000, 2002; Waldhauser et al., 2012). In most cases, splay faults are active and are suspected to play a role in propagating seismic rupture from the plate interface at depth to the surface of the prism (Arai et al., 2016; DeDontney & Rice, 2012; Fisher et al., 2007; Fukao, 1979; Gulick et al., 2011; Moore et al., 2007; Park et al., 2002; Waldhauser et al., 2012). Several questions however remain unanswered. Do interplate seismic ruptures follow only the basal décollement or splay fault(s), or do they partition along the two types of faults? Does rupture propagate at a seismic velocity upward to the surface, or is it damped before reaching the seafloor? Answers to these questions are crucial for seismic and tsunami hazard assessment of seismogenic convergent margins.

For at least four reasons, the Nankai Trough accretionary prism offshore Kii Peninsula (Figure 1) appears as an ideal drilling target to investigate the structure, the evolution, and the mechanical behavior of a splay fault system during large megathrust earthquakes. First, 2-D and 3-D seismic reflection profiles (Moore et al., 2007, 2009; Nakanishi et al., 2008; Park et al., 2000, 2002, 2010; Park & Kodaira, 2012) provide a clear picture of the faults in the prism. 3-D seismic profiles show a basal décollement thrust fault separating the accreted strata from subducting hemipelagic and trench-filling sediments. The basal décollement merges with the top of the basaltic crust about 64-km landward of the deformation front, where the prism thickness is about 8 km. The frontal part of the prism, the so-called “imbricate thrust zone,” includes a series of reverse faults which are interpreted as in-sequence thrusts accommodating plate convergence and allowing frontal accretion. The profiles further show that the splay fault appears as a single strand at depth but divides up-dip into two strands up to ca. 1,400 m apart. Second, inversion of seismic and tsunami waves suggests that the splay fault off Kii Peninsula accommodated, at least partly, the coseismic slip of the 1944  $M_w$  8.2 Tonankai Earthquake and was involved in the genesis of a destructive tsunami (Baba et al., 2006; Baba & Cummins, 2005; Ichinose et al., 2003; Kikuchi et al., 2003; Moore et al., 2007; Satake, 1993; Tanioka & Satake, 2001). Coseismic slip of

the splay fault is also suspected for earthquakes having occurred off Kii Peninsula before the 1944 event. Third, the splay fault off Kii Peninsula is the locus of fluid circulation (Park et al., 2002). More precisely, based on wide-angle and high-density ocean bottom seismograph survey results, Nakanishi et al. (2008) described a thin low-velocity zone along and above the splay fault off Kii Peninsula. In this zone, seismic velocities are 0.5–1.5 km/s lower than in the accretionary prism rocks nearby. By analogy with land-based studies (Kondo et al., 2005; Tsuji et al., 2006), this velocity anomaly reflects the presence of fluids along or near the splay fault (Nakanishi et al., 2008), reinforcing the initial observation by Park et al. (2002). Fourth, the outer part of the Nankai accretionary prism off Kii Peninsula, particularly the area between drilling Sites C0004 and C0007, is recognized as a place where low or very low frequency earthquakes nucleate (Araki et al., 2017; Ito & Obara, 2006; Obara & Kodaira, 2009; Sugioka et al., 2012). Most interestingly, these slow events occur along or close to the splay faults or décollement and correspond to

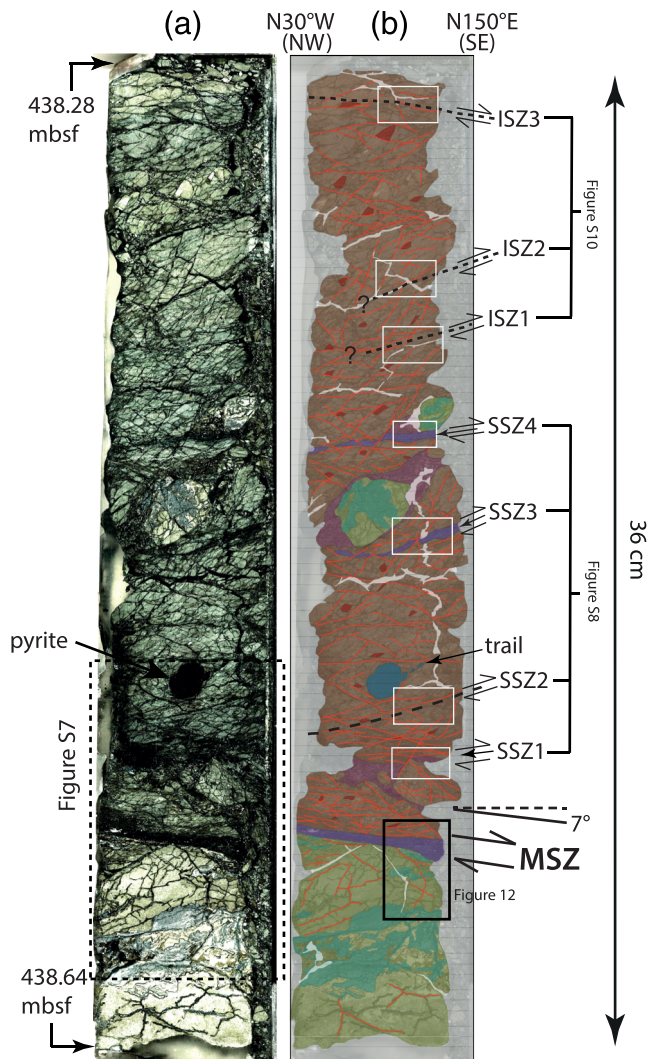


**Figure 3.** (a) Photograph of section 316-C0007D-29R-2 (37–73 cm) from the basal décollement shear zone at Site C0007. (b) Line drawing of (a) with shear zones and location of Figure 12 and Figures S7, S8, and S10 in the supporting information. MSZ: main shear zone; SSZ: secondary shear zone; ISZ: incipient shear zone.

reverse slip. The presence of low to very low frequency earthquakes may be related to the presence of fluids flowing along the various faults in the Nankai prism.

The IODP NanTroSEIZE multiexpedition, multisite drilling program, which started in 2007, aims at a better comprehension of the present structure and the past evolution of the Nankai accretionary prism (Kinoshita et al., 2009; Tobin & Kinoshita, 2006). One major objective of the program is to determine the seismo-mechanical behavior of the major thrust faults that are susceptible to slip during earthquakes and/or to trigger tsunamis. Among the various ways to explore fault mechanics, rock sampling through drilling is an essential method because it allows observation of natural structures. IODP Expedition 316 (Figure 1) recovered cores from the splay fault (Site C0004, Hole C0004D) and from the basal décollement thrust (Site C0007, Hole C0007D) (Kimura et al., 2008; Sreaton et al., 2009). Despite an overall poor recovery, the retrieved cores contain intact millimeter-thick shear zones which are characterized by several types of microstructures. Examination of these microstructures allows one to draw conclusions about the mechanical behavior of the shear zones.

## 2. Geological Setting and Core Treatment

### 2.1. Splay Fault Shear Zone at Hole C0004D

Site C0004 was drilled to cross the splay fault in the Nankai accretionary prism off Kii Peninsula (Kimura et al., 2007; Moore et al., 2007). Hole C0004D (Figure S1 in the supporting information) has a total depth of 400 mbsf (meters below sea floor), of which only the lowermost 300 m were cored, with a recovered core length of 130.76 m (recovery rate of 43.59%). Between 258.01 and 307.52 mbsf, Hole C0004D crossed a zone of fractured and/or brecciated hemipelagic mudstone including frequent thin volcanic ash layers (Unit III, Expedition 316 Scientists, 2009a). The depth of this unit coincides with the location of the lower branch of the splay fault imaged on seismic reflection profiles (Kimura et al., 2008; Kinoshita et al., 2009; Moore et al., 2009). Fracturing and brecciation observed in cores are interpreted as the result of splay fault activity (Kimura et al., 2008; Kinoshita et al., 2009). Several cores containing breccia or gouge zones were recovered (Expedition 316 Scientists, 2009a). However, most of them were significantly disturbed by drilling or by subsequent core

splitting and were therefore of limited interest because of ambiguous deformation structures. The intact recovered section corresponds to the interval 316-C0004D-28R-2,17–49 cm (IODP nomenclature) or the interval between nominal depths 271.08 and 271.40 mbsf (Figure 2). Microfossil and magneto-stratigraphy data indicate a 3.65-Ma age of deposition for the core section above the shear zone and a 1.56-Ma age of deposition for the core section below (Expedition 316 Scientists, 2009a; Kinoshita et al., 2009). This age reversal is interpreted as a consequence of reverse slip along the shear zone.

### 2.2. Basal décollement Shear Zone at Hole C0007D

Site C0007 is located in the frontal part of the prism (Figure 1). Thirty-five cores (Cores 316-C0007D-1R through 35R) were collected from Hole C0007D (Figure S2 in the supporting information) between 175.0 and 493.5 mbsf. The cored length (i.e., penetration) is 318.5 m, and the cumulative recovered core length is 87.9 m (27.6% recovery rate). Three fault zones are observed at 237.5–259.3, 341.5–362.3, and 398.5–446.0 mbsf depths (Kimura et al., 2008; Kinoshita et al., 2009). In these zones, sediments are crossed by polished or striated fault surfaces with <10 cm-spacing of fractures. Occurrence of fault breccia or fault gouge is also observed, with a size of brecciated fragments being ~1–10 mm

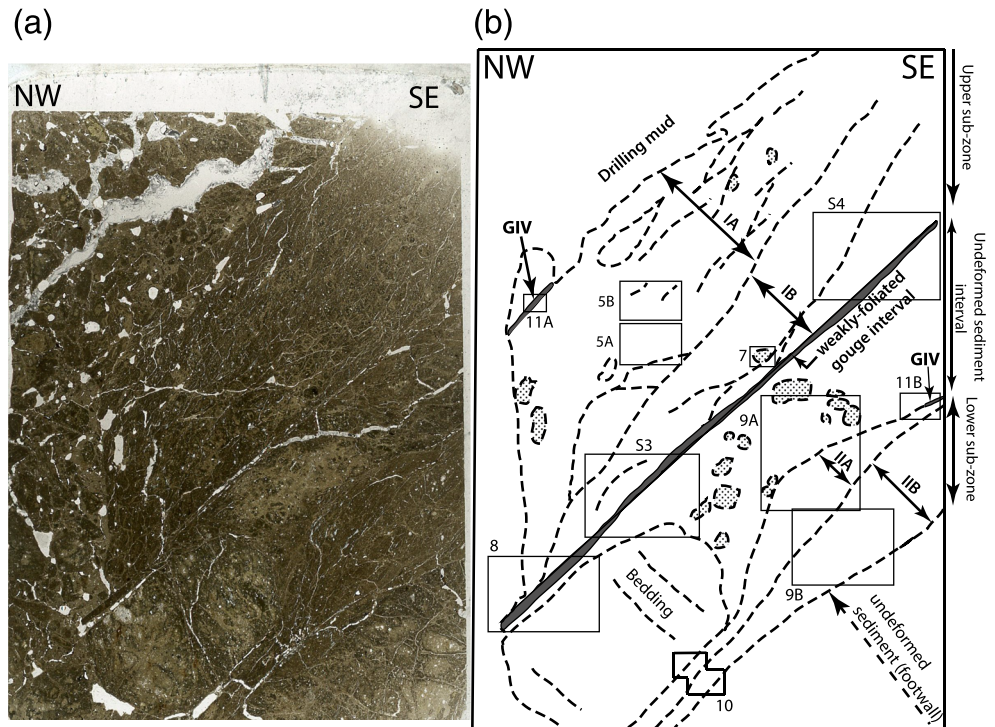


**Figure 4.** Detailed view of the main shear zone preserved in the C0004D splay fault intact core section and showing, from top left to bottom right, the upper subzone, the through-going nonfoliated gouge interval, the undeformed sediment interval and the lower subzone. (a) Scanned image of polished thin section C0004-13 (location in Figure 2). Width is 24 mm. (b) Line drawing of (a), along with locations of Figures 5, 7, 8, 9a, 9b, 10, 11a, and 11b and Figures S3 and S4 in the supporting information. IA: upper, clay-rich, domain of the upper shear zone; IB: lower, clast-rich, domain of the upper shear zone; IIA: upper moderately foliated gouge domain of the lower shear zone; IIB: lower weakly foliated gouge domain of the lower shear zone; GIV: granular injection vein.

(Expedition 316 Scientists, 2009b). The lowermost fault zone separates Pliocene hemipelagic muds and minor ash layers (Unit III, 362.26–439.44 mbsf) from underlying subducted Pleistocene trench turbidites (Unit IV, 439.44–484.44 mbsf) and is interpreted as the basal décollement of the wedge (Kimura et al., 2008; Kinoshita et al., 2009), also referred to as the *plate boundary fault* by Ujiie and Kimura (2014). Within this lowermost fault zone, a 36-cm long intact core (Core 316-C0007D-29R) containing a shear zone was recovered (Figure 3). This core section corresponds to the interval 438.28–438.64 mbsf. The shear zone is located in the lower part of the core, at a depth of 438.57 mbsf, and does not show any disturbance related to drilling or core handling (Expedition 316 Scientists, 2009b). An age reversal was observed between the upper (428.24 mbsf) and the lower (438.61 mbsf) parts of this intact core interval (Expedition 316 Scientists, 2009b). Nannofossils from the upper part suggest a Zone NN12 age (~5.32 Ma), whereas those from the lower part suggest a Zone NN16 assemblage (~3.65 Ma). The time gap between the two dated horizons is estimated at ~1.67 myr (Expedition 316 Scientists, 2009b).

### 2.3. Core Handling and Treatment

For the two holes, shipboard X-ray computed tomography examination of cores allowed selection of two whole-round core section intervals containing millimeter-thick shear zones: 438.28–438.64 mbsf from Hole C0007D (Fig. F32, p. 56, Expedition 316 Scientists, 2009b) and 271.08–271.40 mbsf from Hole C0004D (Fig. F24, p. 50, Expedition 316 Scientists, 2009a). The two core intervals did not undergo the routine shipboard core handling. Instead, given their poor consolidation and the presence of swelling clays, they received a special treatment in order to maintain integrity of the structures and to allow detailed analyses. Using pure ethanol as a cooling fluid, they were first saw-cut longitudinally into three slabs. One slab from each of the two core sections was impregnated with epoxy resin (Epofix®) after drying at 40°C overnight. The

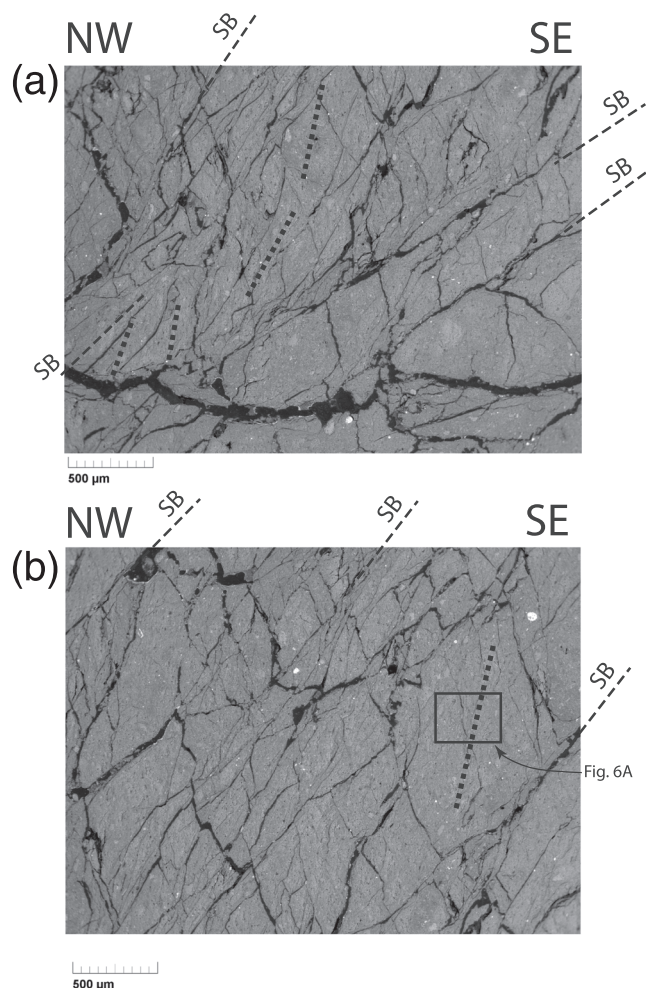


**Figure 5.** SEM images of the upper subzone (location in Figure 4b). (a) Steeply dipping to vertical foliation (dotted lines) deflected by moderately dipping shear bands (dashed lines, SB). The foliation is defined by clay alignment and preferred orientation of elongated clasts. White round dots are framboidal pyrite aggregates. (b) Same as (a), the foliation (dotted line) being steeper in (b) than in (a). Rectangle is the location of Figure 6a.

other two slabs were not impregnated and were kept for long-term storage and for mechanical investigations. The surface of the impregnated slabs was then polished using ethanol. After nondestructive mineralogical and chemical investigations (Hirono et al., 2009, 2014; Sakaguchi et al., 2011; Yamaguchi, Sakaguchi, et al., 2011), the two slabs were cut into chips in order to produce polished thin sections. Again, instead of water, pure ethanol and pure mineral oil were used for chip cutting and thin section polishing. When possible, chips were cut by a hacksaw rather than by an engine-powered rock saw. All thin sections are vertical sections with left-right (L-R) orientations (shipboard scanner references). The ca. 1-cm thickness of the impregnated slabs allowed cutting thin sections in vertical planes perpendicular to the L-R direction. Such additional sections were done only for key microstructures described hereafter. Scanning electron microscopy (SEM) was carried out at University of Strasbourg, France, with a TESCAN Vega II type SEM equipped with an EDAX Pegasus XM4 device for energy dispersive X-ray spectrometry. Thin sections were carbon coated.

#### 2.4. Slab and Thin Section Orientation

Because shipboard routine measurements carried out on and near the intact interval 271.08–271.40 mbsf from Hole C0004D yielded erratic paleomagnetic declination data (Expedition 316 Scientists, 2009a), the intact interval cannot be reoriented with these data. 3D seismic reflection profiles and multibeam bathymetry (Moore et al., 2007, 2009) indicate that the two branches of the splay fault at Site C0004 strike about N60°E and dip N30°W at about 30°. As described below, the C0004 intact core interval shows a shear zone dipping 45 to 50°. If this shear zone is synthetic to the splay faults imaged on reflection profiles, then it should dip toward N30°W. This assumption allows one to attribute the N30°W direction (NW for simplicity) to the R orientation (shipboard scanner references) of the C0004 intact core interval and the N150°E direction (SE for simplicity) to the L orientation. Regarding Hole C0007D, shipboard paleomagnetic declination measurements (Expedition 316 Scientists, 2009b) indicate that the R side (shipboard scanner references) of the 438.28–438.64-mbsf intact interval is toward N150°E (SE for simplicity) and the L side is toward N30°W (NW for simplicity).

### 3. Results From Previous Studies

The two intact core slabs analyzed here and their nonimpregnated counterparts were the subject of mineralogical, geochemical, and mechanical analyses. Vitrinite reflectance measurements within or close to the shear zones indicate significantly higher temperatures than the background temperatures recorded above and below (Sakaguchi et al., 2011). The temperature anomalies are 390°C ( $\pm 50^\circ\text{C}$ ) for the shear zone of Hole C0004D and 330°C ( $\pm 50^\circ\text{C}$ ) for that of Hole C0007D and are interpreted as the results of frictional heating during coseismic slip along the shear zones. This interpretation is strengthened by geochemical analyses which show that the shear zone recovered from Hole C0004D is enriched in Al and K and depleted in Ca and Sr with respect to the overlying and underlying host rocks (Yamaguchi, Sakaguchi, et al., 2011). As in the case of thermal anomalies, these chemical anomalies are interpreted as reflecting a more advanced, temperature-activated, smectite-to-illite reaction in the shear zone. Like the thermal anomalies revealed by vitrinite reflectance, the temperature increase is interpreted to result from coseismic slip-induced frictional heating (Yamaguchi, Sakaguchi, et al., 2011).

In contrast, the investigations carried out by Hirono et al. (2009) suggest that the shear zone sampled at Hole C0004 did not experience temperatures above 300°C. Investigations consisted of inorganic chemical analyses

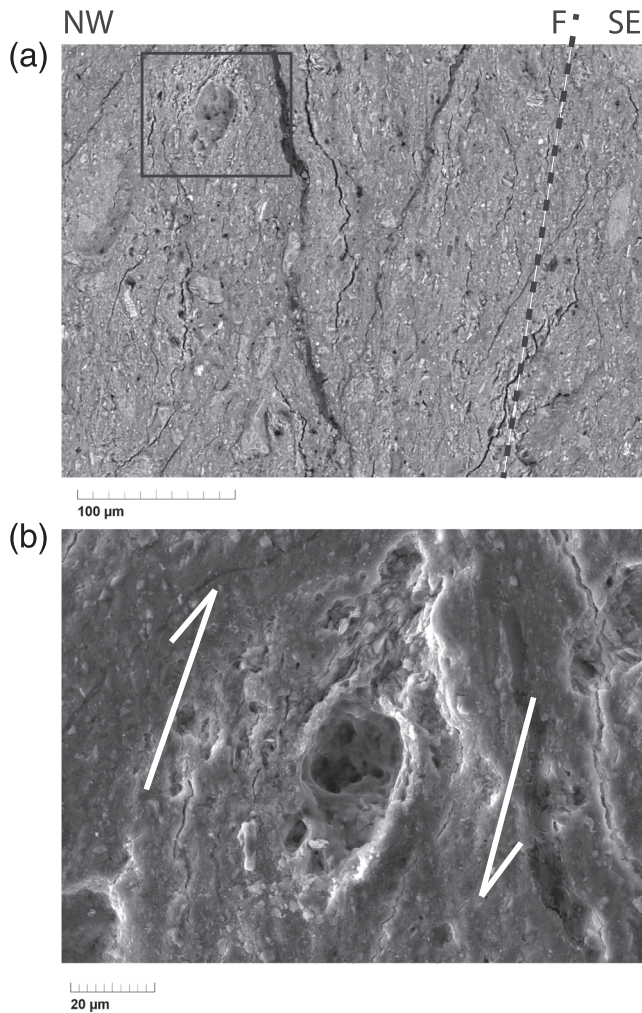


**Figure 6.** SEM images of the foliation and of a porphyroblast system in the uppermost part of the upper subzone. (a) Steeply-dipping to vertical foliation (F) defined by clay alignment and preferred orientation of elongated clasts (location in Figure 5b). (b) Close-up view of a ghost clast flanked by two asymmetrically arranged tails suggesting a reverse sense of shear as indicated by arrows (location in a).

(fluid-mobile trace element concentrations, Sr isotopes), magnetic measurements (magnetic susceptibility and saturation magnetization), inorganic carbon content measurements, and Raman spectroscopy of carbonaceous material. Concentrations of Sr, Cs, Rb, and Li as well as the  $^{87}\text{Sr}/^{86}\text{Sr}$  ratio in the shear zone are not significantly different from those in the host rocks above or below the shear zone, suggesting that the maximum temperature in the shear zone remained below 300°C. Similar conclusions are reached from magnetization measurements, inorganic carbon content measurements, and Raman spectroscopy of carbonaceous material. Additional analyses subsequently carried out on Hole C0004 shear zone by Hirono et al. (2014) consisted of X-ray diffraction spectrometry of the mineral assemblage and infrared spectroscopy of carbonaceous material, along with complementary trace element and isotope compositions. These analyses did not provide any evidence for frictional heating along the shear zone and temperature elevation over the otherwise expected geothermal gradient. Reevaluation of illite formation kinetics by Hirono et al. (2014) furthermore suggests that the high illite-to-smectite ratio in the shear zone may reflect comminution, dissolution, and recrystallization processes during repeated past fault motion rather than a smectite-to-illite reaction thermally activated by a single seismic slip event. Ujiie and Kimura (2014) attempted to reconcile the conflict about the maximum temperature reached along the shear zone at Hole C0004D by pointing out that the empirical relationship between vitrinite reflection and temperature may be less reliable for short duration heating events (such as seismic slip) than for slow events. They conclude that the C0004D shear zone records a heating event, but that the maximum temperature reached during this event is <300°C. Lastly, Hamada et al. (2015) recalculated the slip parameters along the megasplay fault and the basal décollement fault in order to fit vitrinite reflectance data obtained by Sakaguchi et al. (2011) with kinetic models. Their analysis suggests that the maximum temperature recorded in the gouge zones of the two faults is about 340°C and was reached after rise times of 6,250 s along the megasplay fault and of 2,350 s along the décollement fault. Such rise times, which are surprisingly long (40 min to 1.5 hr), are more typical of slow earthquake-like event durations than of standard earthquake durations.

In addition to these investigations devoted to tracking possible coseismic heating imprints along or near Hole C0004D or Hole C0007D shear zones, low to high velocity shear experiments were carried out to determine the

frictional properties of the gouges constituting the intact shear zones. Gouges from C0004D and C0007D shear zones were tested at low (0.03–100 μm/s; Ikari et al., 2009; Ikari & Saffer, 2011), moderate (0.0026–260 mm/s, Tsutsumi et al., 2011), and high velocities (1.3 m/s slip rate; Ujiie & Tsutsumi, 2010). At low velocities (Ikari & Saffer, 2011; Ikari et al., 2009), gouge samples from Sites C0004 and C0007 are characterized by velocity-strengthening frictional behaviors, indicating stable sliding and ruling out the nucleation of earthquakes along the splay fault or along the décollement fault. However, for all tested samples, the minimum values of the rate-and-state friction law constitutive parameter (a-b) are observed at sliding velocities of ca. 1–3 μm/s, corresponding to 0.1–0.3 m/day, which is close to the slip velocity of low-frequency events recorded nearby (Araki et al., 2017; Ito & Obara, 2006; Obana & Kodaira, 2009; Sugioka et al., 2012). At intermediate velocities, Tsutsumi et al. (2011) show that both velocity-strengthening (stable sliding) and velocity-weakening (potentially unstable sliding) are observed, suggesting a more complex behavior of the gouge zones than interpreted by Ikari et al. (2009) or by Ikari and Saffer (2011). Additionally, the samples characterized by velocity-strengthening behavior show that the deformation is homogeneously distributed over the entire shear zone, while those characterized by slip-weakening show that the deformation is heterogeneous and is localized along narrow shear zones (Tsutsumi et al., 2011). High-velocity friction experiments

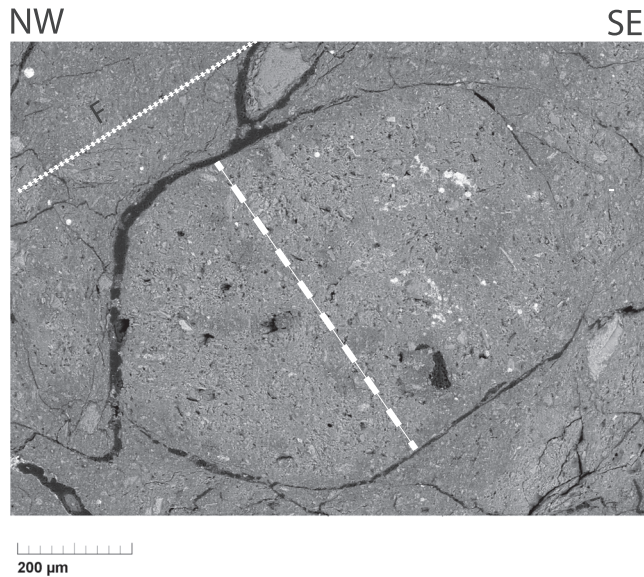


**Figure 7.** SEM image of a well-rounded siltstone clast in the clay-poor part of the upper subzone (location in Figure 4b). The bedding trace (white dashed line) inside the clast is at high angle to the general trend of the foliation in the surroundings of the clast (white dotted line), indicating rotation of the clast.

conducted by Ujiie and Tsutsumi (2010) on water-saturated clay-rich material from Hole C0004D gouge-hosting rocks are characterized by slip-weakening as indicated by a low peak friction, a low steady-state friction, a very small slip-weakening distance, and a very small fracture energy. The weakening, which is interpreted as the result of thermal pressurization (e.g., Faulkner et al., 2011), suggests that earthquake ruptures from deeper parts of the splay fault or of the plate interface can readily propagate along the clay-rich gouge zones recovered from the shallow parts of the splay fault.

#### 4. Splay Shear Zone Microstructural Analysis

The splay fault zone intact core section from 271.08 to 271.40 mbsf (Figures 2 and 4) shows a main shear zone (MSZ) and two secondary shear zones (SSZs) ca. 3.2 cm above the MSZ. The shear zones consist of foliated gouge. Nonfoliated or weakly foliated gouge is also observed, either outlining sharp fault surfaces or in the form of injected gouge. A description of these objects, based on optical microscope and SEM observations, is given in the following section.

##### 4.1. Main Shear Zone

The MSZ preserved in the C0004D intact core section consists of two discrete shear zones: an *upper subzone* crossing the entire core and whose ca. 8-mm thickness is constant and a *lower subzone* whose thickness varies between 1 and 5 mm and which tapers upward and southeastward

(Figure 2). The two subzones are parallel, dip  $45^\circ$  northwestward and are separated by an interval of undeformed sediment whose thickness is between 3.6 and 6.6 mm. A polished thin section encompassing the MSZ (Figure 4) shows that the upper subzone is limited at its base by a thin and planar *weakly foliated gouge interval* which can be traced across the entire thin section.

##### 4.1.1. Upper Subzone

Optical microscope and SEM observations show that the upper subzone consists of a foliated gouge composed of an upper clay-rich (i.e., clast-poor) domain and a lower clast-rich (i.e., clay-poor) domain (Figure 4, domains IA and IB). In the upper clay-rich domain IA (Figure 5), the poorly to well-marked foliation dips steeply ( $70^\circ$ ) northwestward or is vertical, but its overall trace undulates. The foliation is defined by the alignment of clay particles and elongated clasts (mostly plagioclase). It is truncated and deflected by moderately to steeply dipping shear bands (Figure 5). The combination of the foliation and the shear bands defines a composite planar fabric (Chester & Logan, 1987; Rutter et al., 1986). The shear band dip angles are between  $40^\circ$  and  $70^\circ$  to the northwest, similar to the shear zone. Some of the shear bands appear as open cracks whose inner walls are sporadically decorated with pyrite aggregates. The aggregates are too small to determine whether the crystals are framboidal, euhedral, or anhedral. The deflection of the foliation by the shear bands consistently indicates a reverse sense of shear (Figure 5). This reverse sense of shear is confirmed by a partly preserved porphyroclast-tail system (Figure 6). The clast itself is no longer present (possibly detached during thin section polishing), but asymmetrical clay particle tails around the clast ghost indicate a reverse sense of shear. The lower clast-rich domain IB is poorly foliated. The foliation is developed along clast-free rectilinear intervals dipping  $45^\circ$  northwestward. The foliation never penetrates the clasts but rather abuts against or wraps around them. Clasts are rounded and not fractured. The relict bedding surface inside some clasts shows that they underwent rotation after incorporation into the shear zone (Figure 7). Where foliation is developed, it dips  $30\text{--}50^\circ$  and tends to become parallel to the weakly foliated gouge interval where close to it. The foliation of domain IB is clearly deflected or truncated by the weakly foliated gouge interval.

##### 4.1.2. Weakly Foliated Gouge Interval

The *weakly foliated gouge interval* at the bottom of the upper subzone is about 0.4 mm thick and is bounded by two fault surfaces. Locally, where the two fault surfaces merge, the gouge is either absent or too thin to be distinguished, even at SEM scale. The upper fault surface, which separates the weakly

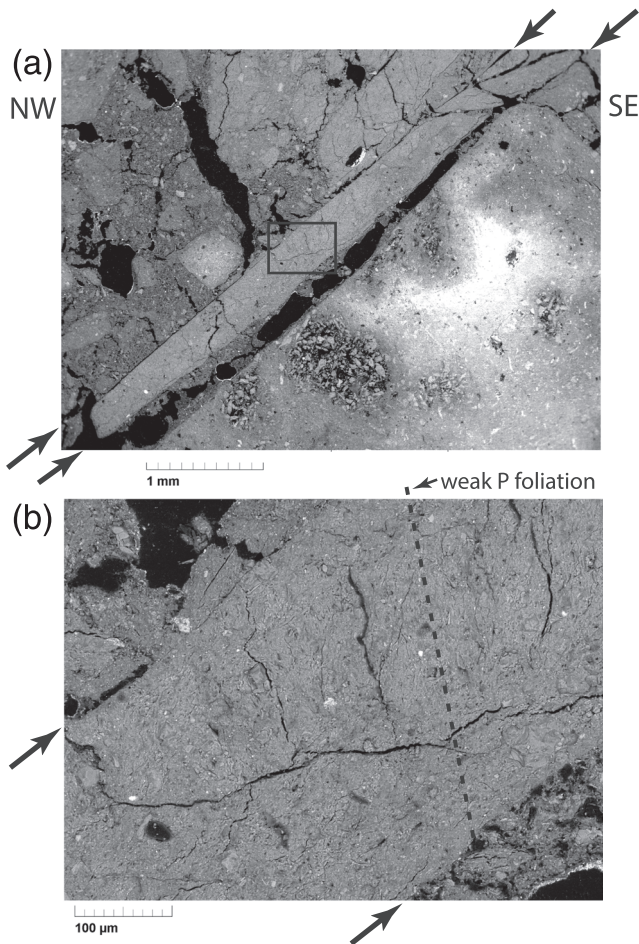


**Figure 8.** SEM images of the weakly foliated gouge interval in the lower part of thin section C0004-13. (a) Overview of the central weakly foliated gouge interval (location in Figure 4b). Arrows indicate the boundaries of the interval. (b) Close view of the central weakly foliated gouge (location in a). Arrows indicate the boundaries of the interval.

matrix is composed of clay particles along with abundant detrital mineral grains (quartz and feldspar) and minor volcanic shards, pumice clasts, and bioclasts. No bedding can be recognized in the matrix. However, the longest axis of some volcanic shards or of detrital grains with large aspect ratios is parallel to the overlying fault-bound gouge interval, possibly reflecting some degree of reorientation during deformation. Bedding is preserved in the largest clasts (Figure 4b), but its orientation is not constant, indicating that the clasts underwent rotation. Compared with the overlying upper subzone or the underlying lower subzone, the matrix is not foliated. Particularly, clay particles do not show any preferred orientation.

#### 4.1.4. Lower Subzone

The *lower subzone* consists of a foliated clayey gouge including angular fragments of quartz, feldspar, and bioclasts. Most fragments are internally fractured. No clast larger than 100  $\mu\text{m}$  can be observed, indicating a significant size reduction with respect to the clasts in the overlying or underlying sediments. The clast size reduction in the lower subzone is not as advanced as in the through-going weakly foliated gouge interval described above. Indeed, the mean size of the clasts in the lower subzone gouge is about 20  $\mu\text{m}$ , whereas it is about 5  $\mu\text{m}$  in the weakly foliated gouge interval. SEM images show that the foliated gouge is more compact than the overlying or underlying sediment intervals. In particular, voids are less numerous and smaller (Figures 9 and 10).

foliated gouge from the upper gouge, is finely striated. The striation is perpendicular to the strike of the surface, indicating a pure dip-slip motion. Epoxy impregnation prevents checking whether the lower fault surface is striated or not. The weakly foliated gouge interval (Figure 8 and Figures S3 and S4 in the supporting information) shows the following characteristics. (1) The matrix is made of a mixture of clay particles and small ( $\sim 1\mu\text{m}$ ) clasts. (2) The clasts consist of quartz, feldspar, chlorite, and bioclasts. (3) Clasts are angular and have significantly smaller sizes (between 1 and 10 $\mu\text{m}$ , 50 $\mu\text{m}$  for the largest ones) than their counterparts outside (mostly larger than 50 $\mu\text{m}$ ). Clasts of quartz or feldspar are intensely fractured. (4) Large (length  $>30\mu\text{m}$ ) clasts with high length-to-width ratios tend to be aligned parallel to the fault surfaces bounding the interval. Conversely (Figures S3 and S4 in the supporting information), the alignment of small (length  $<20\mu\text{m}$ ) clasts with high length-to-width ratios defines a second foliation steeper than the previous one. This weak foliation is oblique to the interval in an anticlockwise geometry. It can be interpreted as an internal P foliation (Figure 8 and Figures S3 and S4 in the supporting information). (5) There is no evidence for any relict sedimentary layering. (6) Despite numerous open cracks (possibly linked to sample handling or preparation), the weakly foliated gouge interval is more compacted than the surrounding foliated gouge domain above or the intact sediment below. This compaction is manifest in a lighter gray shade of the weakly foliated gouge with respect to that of the surrounding material (foliated gouge above or intact sediment below). Framboidal pyrite aggregates observed in the weakly foliated gouge do not show evidence for any deformation (e.g., fracture), suggesting either that they crystallized *after* deformation or that they crystallized *before* deformation but escaped comminution during gouge formation because they were harder than the surrounding sediments.

#### 4.1.3. Undeformed Sediment Interval

Between the weakly foliated gouge interval and the lower subzone of the MSZ of the splay fault (Figure 4) lies an interval of undeformed sediment. It consists of rounded clasts embedded in a clayey matrix. The largest clast has a 7.2 mm  $\times$  14.4 mm size. The largest dimension of other clasts does not exceed 1.2 mm. The clasts consist of silty clay. The

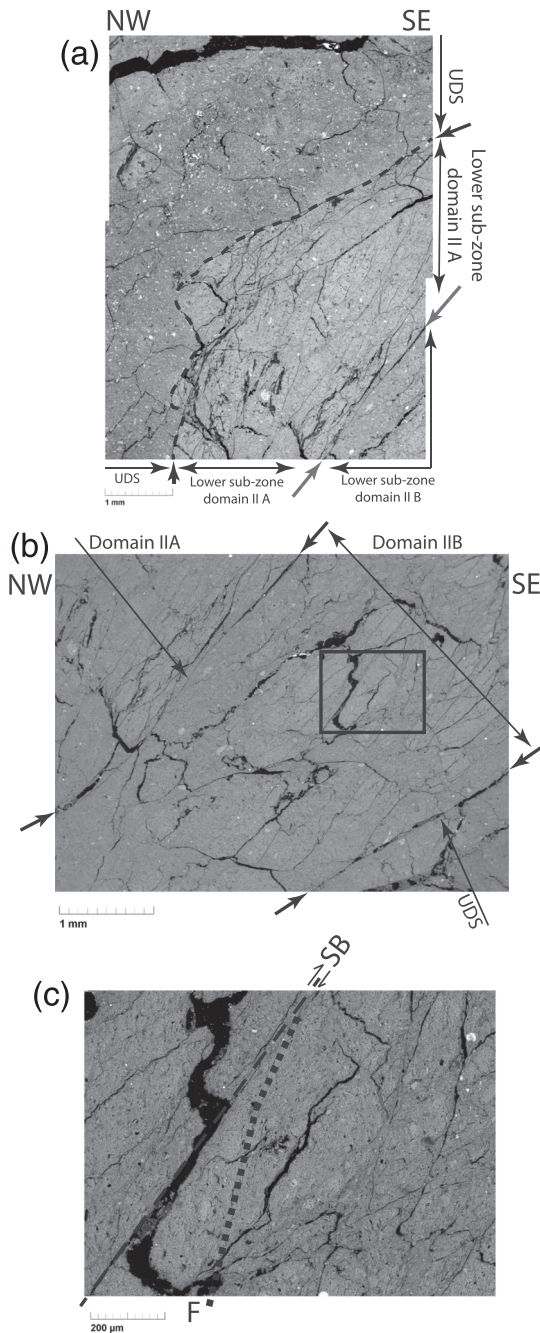


**Figure 9.** (a) Composite SEM image showing a part of the lower subzone of thin section C0004-13 (location in Figure 4b). The lower subzone consists of an upper domain IIA composed of a foliated clayey gouge and a lower domain IIB composed of a moderately foliated clayey gouge. UDS: overlying undeformed sediment. Note the sharp but irregular trace of the boundary between domain IIA and the overlying sediment, suggesting intrusion of the former into the latter. Red arrows indicate the sharp and rectilinear trace of the boundary between domains IIA and IIB. (b) SEM image of the lower subzone showing, from top right to bottom left, the foliated gouge (domain IIA), the moderately foliated gouge (domain IIB), and the footwall undeformed sediment (UDS). Arrows indicate boundaries between the three domains. Location in Figure 4b. (c) Closer view of the domain IIB moderately foliated gouge showing deflection of the steeply (close to vertical) dipping foliation (F) by shear bands (SB).

Two domains can be distinguished in the lower subzone (Figure 4): an upper foliated, domain IIA, and a lower moderately foliated, domain IIB. The trace of the boundary between the foliated gouge domain IIA and the overlying intact sediment interval is sharp and strongly undulating (Figure 9a). Such an irregular shape of the boundary suggests that the domain IIA “indented” the intact sediment interval, after formation of the lower shear zone. The boundaries between domains IIA and IIB and between domain IIB and the underlying undeformed sediment are also sharp and planar or slightly undulating (Figures 9 and 10). Unlike the uppermost boundary, they seem to be undeformed. Domain IIA is between 0.6 and 3 mm thick and is characterized by a foliation mostly visible in clay-rich domains and absent in domains where clasts are abundant. Overall, the foliation trace is irregular, discontinuous and seems to abut against fractures dipping  $45^\circ \pm 5^\circ$  northwestward. These fractures are possibly shear bands, but offset of foliation is not obvious. Domain IIB is between 0.6 and 4.2 mm thick and consists of a moderately developed foliated fault gouge (Figures 9 and 10). The foliation is less developed than in domain IIA. Deflection of the foliation along shear band-like fractures near the boundary with domain IIA indicates a top-to-the-SE reverse sense of shear (Figure 9c). The sporadic presence of framboidal or isolated pyrite along the boundaries between the lower shear zone and the surrounding sediments or along fractures inside the shear zone (Figures 9 and 10) provides evidence for fluid flow possibly after formation of the lower subzone.

#### 4.1.5. Injected Nonfoliated Gouge

In the upper left (northwestern) corner of the upper subzone (Figures 4b and 11a), a fine and compact nonfoliated gouge fills a 2-mm long and 200-μm wide interval crossing poorly foliated gouge of the upper subzone domain IA. The grain size is unimodal and varies between 5 and 10 μm. The boundaries between the nonfoliated gouge and the host gouge are not rectilinear but irregular. This type of boundary, which is preserved in the fragment at the center of the image, precludes any slip along the boundary but rather suggests a dilational opening and filling with the nonfoliated gouge. In addition, the characteristics (color, nature, size, and angularity of fragments and compaction) of the filling gouge are similar to those of the non-foliated gouge observed along the through-going fault (Figure 8b and Figures S3b and S4b in the supporting information). This gouge vein can tentatively be interpreted as a granular injection vein as defined by Rowe et al. (2012) or by Smeraglia et al. (2016). Due to the proximity between the two features (8.7 mm), this injection vein could be linked with slip along the through-going fault. The gouge filling the vein would have been injected from the weakly foliated gouge of the through-going interval. An alternative interpretation is that the material filling the vein comes from the surrounding sediment, as observed in vein structures (Cowan, 1982). However, this interpretation is unlikely, because vein structures were not observed in any of the other 12 thin sections prepared from the C0004D intact slab.

A similar dilational vein filled with fine homogeneous nonfoliated gouge, and tentatively interpreted as a granular injection vein, is observed in the upper right part of the lower subzone, along the boundary between domain IIA and the overlying undeformed sediment (Figures 4b and 11b). The gouge shows the same grain size as the vein described above

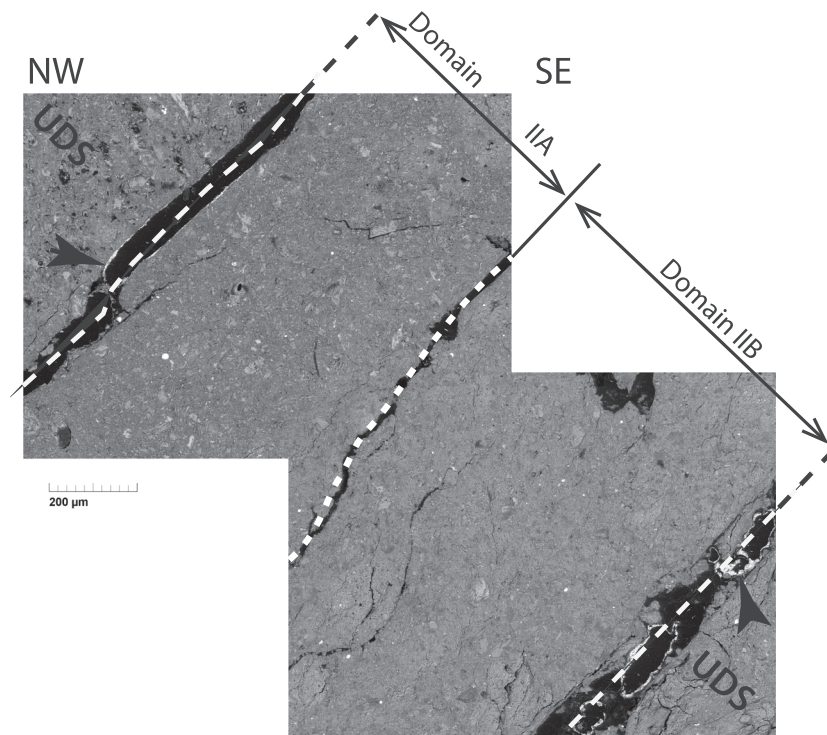


**Figure 10.** Composite SEM image showing the contact between domains IIA and IIB of the lower subzone (location in Figure 4b). UDS: undeformed sediment. Arrow indicates pyrite coating on the walls of voids along the boundary with UDS.

and displays a similar gray shade, suggesting a similar density. The lower boundary of the vein is truncated by the fault surface separating the lower shear zone from the overlying undeformed sediment.

#### 4.2. Secondary Shear Zones

About 3.2 cm above the MSZ (ca. 260 mbsf), two SSZs are observed in an otherwise intact sediment (Figures S5 and S6 in the supporting information). These shear zones dip about 20–25° northwestward. The upper shear zone consists of a nonfoliated gouge characterized by a reduction of the size of the clasts inside the zone with respect to that of the clasts outside (Figure S6a in the supporting information). The lower shear zone consists of a weakly foliated gouge. The weakly marked foliation is defined by an alignment of clay particles and of elongated clasts (Figure S6b in the supporting information) and is interpreted as a P foliation. The obliquity of the P foliation relative to the shear zone boundaries suggests a top-to-the-SE reverse sense of slip. No SSZ could be detected elsewhere in the intact core slab thin sections.

### 5. Basal Décollement Microstructural Analysis

The intact interval of the basal décollement fault zone (Figure 3; interval 316-C0007D-29R-2,37–73 cm; 438.28–438.64 mbsf) shows a MSZ separating intensely fractured green hemipelagic mudstone in the hanging wall from weakly fractured green siltstone with intercalations of gray ash in the footwall (Expedition 316 Scientists, 2009b). The ca. 1.67 myr time inversion mentioned above (see section 2.2) is observed between the two walls of the MSZ. The bedding surface is recognizable in the footwall siltstone, whereas it is not recognizable in the hanging-wall mudstone. Four SSZs (numbered from 1 to 4) and three incipient shear zones (ISZs) (numbered from 1 to 3) can be identified in the hanging-wall mudstone (Figure 3).

#### 5.1. Main Shear Zone

The MSZ (Figures 3, 12, and 13 and Figure S7 in the supporting information) consists of a 2- to 10-mm thick foliated clay gouge dipping 7–8° southeastward. Upward, the otherwise well-marked and regularly spaced foliation of the MSZ progressively loses its regularity and lateral continuity before disappearing in the

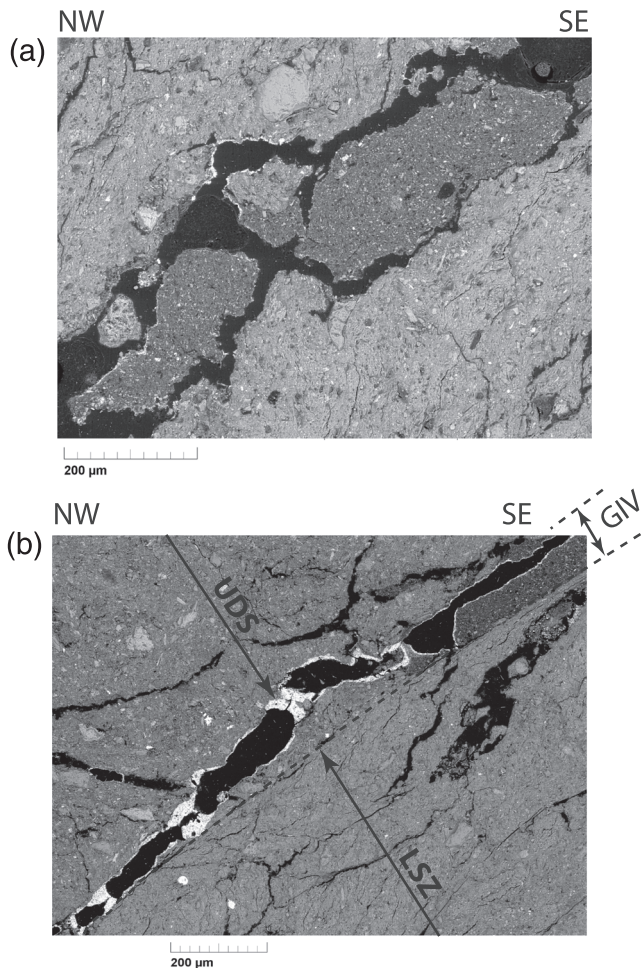


**Figure 11.** SEM images of dilational veins filled with fine homogeneous nonfoliated gouge and tentatively interpreted as granular injection veins. (a) SEM image of a dilational vein filled with gouge observed in the upper left part of thin-section C0004-13, above the upper shear zone (location on Figure 4a). (b) SEM image of a dilational vein filled with gouge observed at the top right of the lower subzone (location in Figure 4b). The lower boundary of this vein is truncated by the sharp plane separating the lower subzone (LSZ) from the overlying undeformed sediment (UDS). GIV: granular injection vein. White coating on the walls of open cracks consists of pyrite crystals.

intact sediment. Between the MSZ and the intact sediment, the transition domain, 6.5- to 7.5-mm thick is visible on both NW-SE and perpendicular NE-SW thin sections (Figures 12 and 13 and Figure S7 in the supporting information). Downward, the MSZ is truncated by an undulating fault surface by which the foliated gouge is in contact with the underlying intact sediment through a brecciated interval (Figure 14). A redox front delineated by a rim of isolated or aggregated iron sulfide crystals in the intact footwall is also truncated by the fault (Figure 14).

The MSZ is characterized by a composite planar fabric combining foliation and shear bands (Figure 15; Chester & Logan, 1987; Rutter et al., 1986). The foliation is defined by alignment of clay particles and clasts with aspect ratios larger than 2:1. SEM energy-dispersive X-ray spectroscopy analyses indicate that the clay consists of mixed illite-smectite. The clasts are rarely larger than 100  $\mu\text{m}$ , most of them having sizes between a few microns and 40  $\mu\text{m}$ . They are angular and fractured, suggesting a mechanical fracturing process (comminution or attrition). SEM energy-dispersive X-ray spectroscopy analyses allow identification of quartz, feldspar, and chlorite clasts. Framboidal pyrite aggregates are also observed. No bioclast could be found, possibly because intense fracturing prevents their recognition. The foliation dips 5–15° northwestward and is deflected by shear bands along which clay particles align parallel to the bands (Figure 15). Shear bands often appear as open cracks, possibly resulting from clay contraction following drying or epoxy impregnation. The foliation-shear band relationship indicates a noncoaxial top-to-the-SE shear deformation (Figure 15). The acute angle between the foliation and the shear bands decreases downward from about 35° in the upper part of the transition domain to about 20° or less in the lower part of the MSZ, suggesting a downward increase in shear strain. On the NE-SW vertical thin section (Figure 13) prepared in the same chip as the one for C0007-35 NW-SE thin section but perpendicular to it, the foliation surfaces and the shear bands have variable dip angles and dip directions, and no clear cross-cutting relationship between the two surfaces can be established. Foliation surfaces and shear bands show consistent relationships in the NW-SE vertical plane (Figures 12 and 15) and inconsistent relationships in the NE-SW vertical plane (Figure 13). This suggests that the NW-SE vertical plane is likely closer to the X-Z plane of the strain ellipsoid while the NE-SW vertical plane is likely closer to the Y-Z plane of the strain ellipsoid, X, Y, and Z being the principal axes of the strain ellipsoid, with X being the axis of maximum elongation, Z being the one with minimum elongation, and Y being the intermediate axis (Passchier & Trouw, 2005).

As mentioned above, the lower boundary of the MSZ is a planar to gently undulating fault surface by which the foliated gouge above is in contact with the intact sediment below (Figures 12, 13, and 14). Above the fault surface, the foliated gouge is brecciated over a thickness not exceeding 200  $\mu\text{m}$  (Figure 14). The microbreccia was formed at the expense of the overlying foliated gouge. A strongly undulating redox front, marked by tiny (about 20  $\mu\text{m}$  long) subhedral to anhedral pyrite grains, is preserved in the footwall intact sediments but is also truncated by the fault. Although less abundant than below the redox front, some pyrite crystals are present above the front and below the fault. In the lower right part of Figure 14a, a large (0.35 mm long) elliptical aggregate of pyrite is preserved above the front. It is flanked by a tail of tiny crystals indicating stretching parallel to the overlying fault.

## 5.2. Secondary Shear Zones

Four SSZs numbered from 1 to 4 are found 1.5, 3, 5.5, and 7.5 cm above the MSZ (Figure 3 and Figure S8 in the supporting information). These SSZs, which can be identified visually on the core because of their

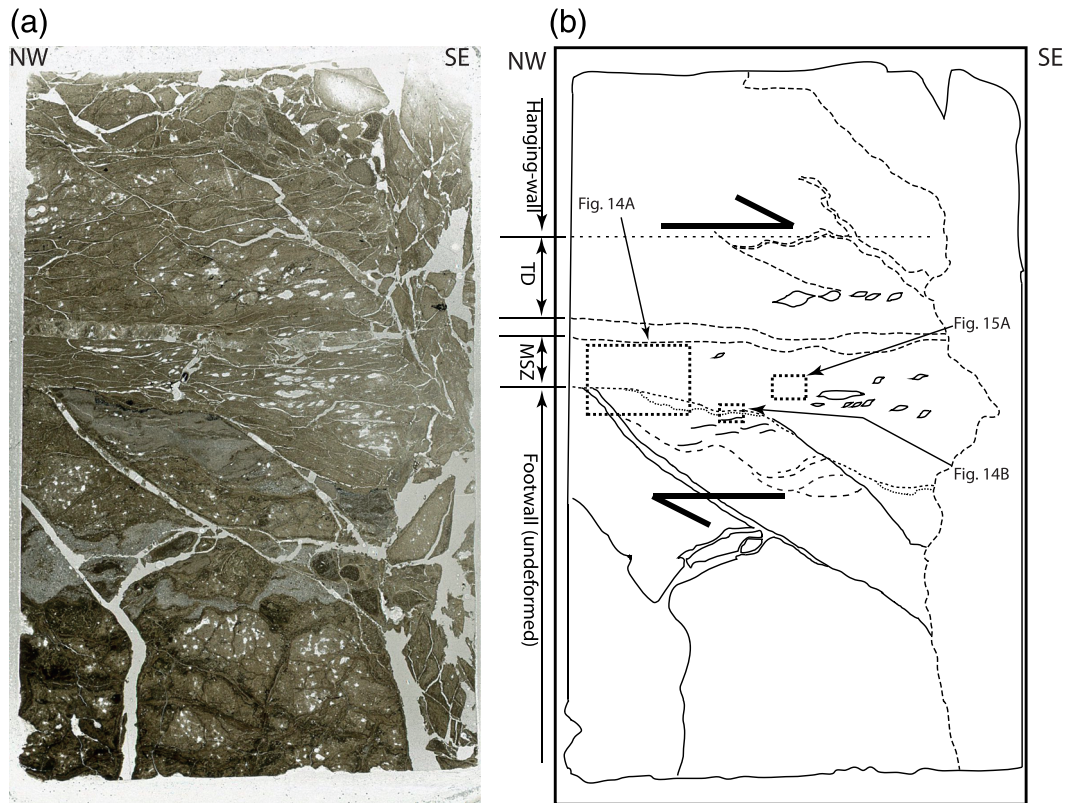


**Figure 12.** (a) Scanned image of polished thin section C0007-35 (location in Figure 3). Width is 24 mm. (b) Line drawing of (a), along with locations of Figures 14a, 14b, and 15a. MSZ: main shear zone; TD: transition domain. The undulating dotted line beneath the MSZ is the redox front. Sense of shear inferred from foliation-shear band relationships in the MSZ is top-to-the-SE.

compact aspect and darker color, are thinner than the MSZ below and dip  $3\text{--}21^\circ$  in the direction opposite to that of the MSZ. Each of these zones is composed of foliated gouge showing the same composite characteristics as observed in the MSZ (Figure S9 in the supporting information). The foliation-shear band relationship consistently indicates a top-to-the-SE sense of shear, as for the MSZ.

### 5.3. Incipient Shear Zones

Three ISZs, numbered from 1 to 3 (Figure 3 and Figure S10 in the supporting information), are located above the previously described SSZs. They are located 9, 10, and 14 cm above the MSZ. They are thinner than the SSZs below and cannot be identified visually on the core. Optical microscope observation of thin sections is required for detection. The ISZs dip either southeastward or northwestward with dip angles between  $8^\circ$  and  $20^\circ$ . Within these three zones, the foliation is weakly developed and less regular than within the secondary zones below (Figure S11 in the supporting information). Poorly developed shear bands slightly offset the foliation, indicating the same shear sense as those observed along the MSZ and SSZs below (Figure S11 in the supporting information).

## 6. Discussion

The two intact shear zones studied here may constitute only a fraction of the shear zones crossing the Nankai prism at Sites C0004 and C0007. However, the age reversals observed across them demonstrate that they accommodated significant displacements. This suggests that the shear zones can be regarded as representative of the fault zone rocks and microstructures in the Nankai prism. The various microstructures observed in the two intact shear zones are summarized in Figure 16.

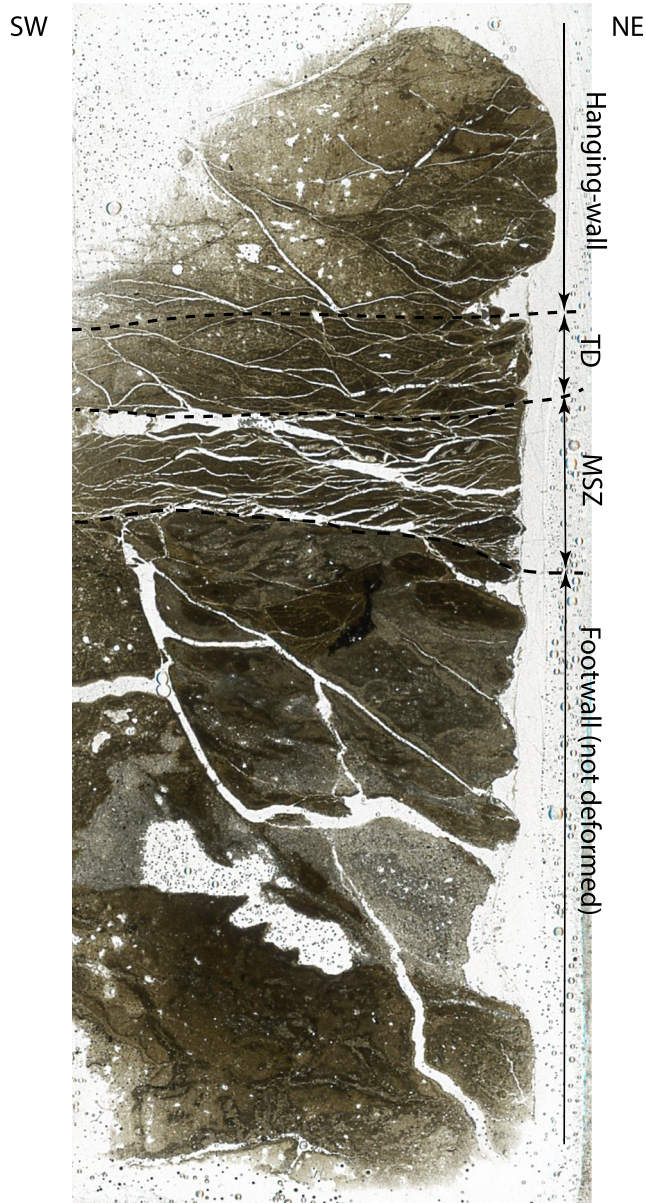


**Figure 13.** Scanned image of the NE-SW-oriented thin section perpendicular to thin section C0007-35 and showing parallelism between foliation and shear band within the main shear zone (MSZ). TD: transition domain.

### 6.1. Relative Chronology of the Various Microstructures

In the splay fault intact core section (Figures 2 and 4), based on the observed microstructures and mutual relationships between them, several chronologies of deformation are proposed. In the *upper subzone*, the formation of the foliation and the associated shear bands in domains IA and IB predates the formation of the through-going fault zone and associated weakly foliated gouge interval. In the *lower subzone*, the weakly foliated gouge of domain IIA was formed before the formation of underlying domain IIB gouge, based on cross-cutting relationships. Given the limited size of the core, it is not possible to establish relative chronologies between deformation events in the upper subzone and those in the lower subzone. Regarding the décollement intact core section, the formation of the flat-lying sharp fault surface and of the associated microbreccia post-dates the formation of the MSZ and of the underlying redox front.

### 6.2. Kinematics

Along the MSZ of the splay fault intact core section (Figures 2 and 4), the sense of displacement can be ascertained within the upper subzone (domains IA and IB) as well as within the lower subzone (domain IIB). For both shear zones, shear band/foliation relationships indicate a reverse top-to-the-SE shear sense (Figures 5, 6, and 9c). The sense of displacement along the fault surfaces bounding the through-going gouge interval remains undetermined. The obliquity of the P foliation inside the nonfoliated gouge, with a counterclockwise geometry (Figures S3 and S4 in the supporting information), suggests a reverse sense of shear. Regarding the two SSZs observed above the C0004D MSZ, the lower one shares the same reverse top-to-the-SE shear sense (Figures S5 and S6b in the supporting information). If the hypothesis regarding the orientation of the C0004D intact interval (see section 2.4) is correct, the reverse sense of shear is top toward N150°E, in agreement with the regional tectonic setting. Along the MSZ of Site C0007 basal décollement intact core interval (Figure 12 and Figure S7 in the supporting information), the sense of shear is well documented by the foliation/shear band relationship and is consistently top-to-the-SE, here also in agreement with the regional tectonic context.

The SSZ and ISZ overlying the MSZ of the Hole C0007 intact core interval are likely secondary fault surfaces related to displacement along the MSZ. There is a clear upward decrease in deformation intensity from the basal MSZ to the uppermost ISZ3. Given their inclination with respect to the MSZ and given their kinematics, all SSZ and ISZ except ISZ3 can be interpreted as undulating Y shear zones (Figure 17; Logan et al., 1992; Mandl et al., 1977; Swanson, 1988; Tchalenko, 1968).

### 6.3. Relating Microstructures to Slip Rate: Cautionary Notes and Hypotheses

The fault rocks observed in the two intact core intervals from Sites C0004 and C0007 are of two types: moderately foliated or foliated gouge on one hand and weakly foliated gouge and microbreccia on the other hand (Figure 16). Relating these fault rock types to contrasted strain rates (rapid deformation vs. slow deformation) is tempting but should be done with caution. Indeed, the observed fabrics could also reflect differences in consolidation state when the material was deformed. In particular, an overconsolidated material will behave in a brittle manner, while a material under compaction may behave in a ductile manner for the same strain rate. Moreover, even in the case of a strain rate interpretation, there is a difference between coseismic rates and imposed rates that are too fast to be accommodated by ductile processes. Despite these difficulties, the following hypothetical correlations are proposed.

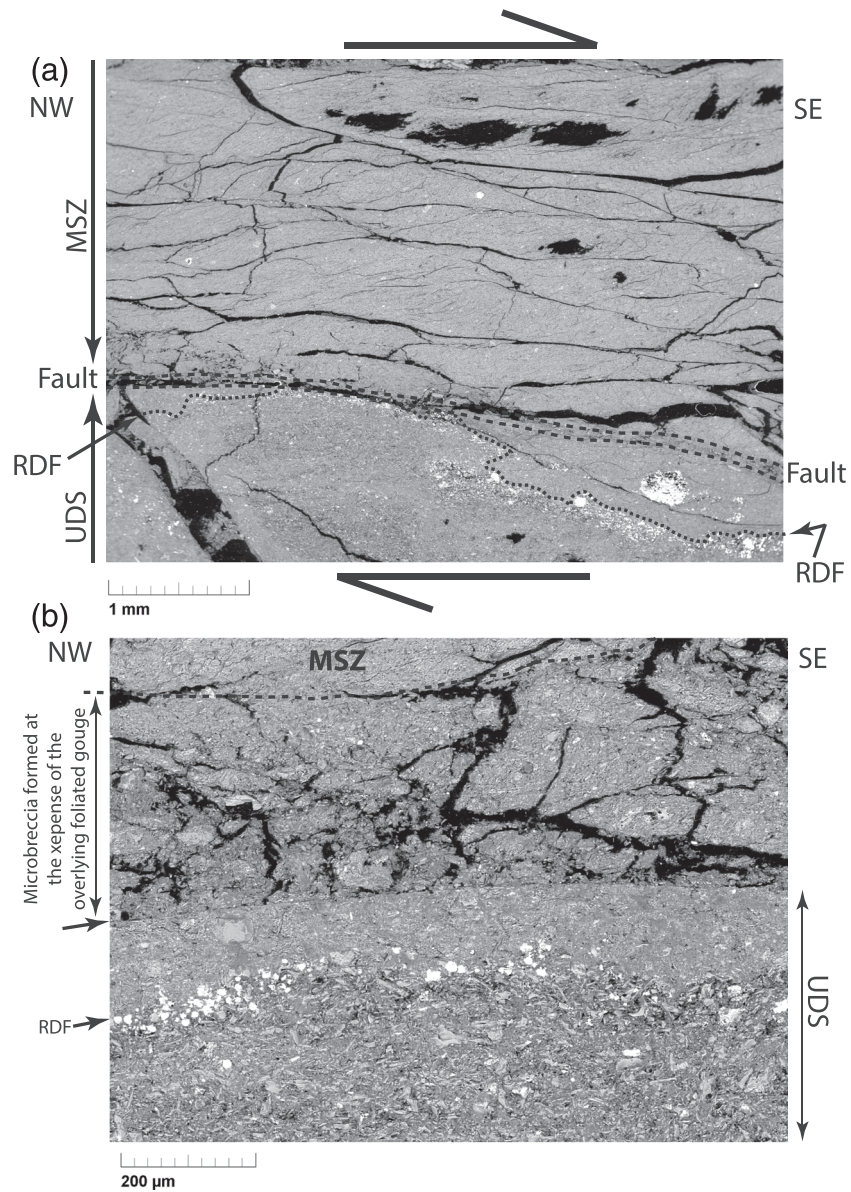


**Figure 14.** (a) SEM image of the faulted boundary (fault) between basal décollement main shear zone (MSZ) and footwall undeformed sediment UDS (location on Figure 12). RDF: redox front between the MSZ foliated gouge and the footwall undeformed sediment. Isolated or aggregated whitish dots are iron sulfides. The composite planar fabric (foliation F/shear band SB) in the MSZ indicates a top-to-the-SE sense of shear, but loses its regularity and coherency downward near the faulted boundary. (b) Enlarged view of the MSZ-UDS faulted boundary (location on Figure 12). Arrow at the top of the undeformed sediment (UDS) points at the sharp boundary fault surface.

The presence of foliated gouge in a fault zone is interpreted as the result of a slow, typically aseismic deformation (Chester et al., 2004; Chester & Chester, 1998; Miller, 1996; Scholz, 2002; Sibson, 1977). This interpretation also agrees with rock shear deformation experiments at room temperature showing that foliation forms under low shear rates (Reinen, 2000; Saito et al., 2013). By analogy with these studies, it is reasonable to consider the foliated gouge observed along the upper and lower subzones of the C0004D MSZ as well as along the C0007 basal décollement zone or along the SSZs above them to be the result of aseismic displacement, either at creep rates (cm/year) or at afterslip or slow slip event rates (cm/day to cm/week). Conversely, the through-going weakly foliated gouge interval observed in the MSZ of the C0004D intact core section (Figures 4 and 8 and Figures S3 and S4 in the supporting information) cross-

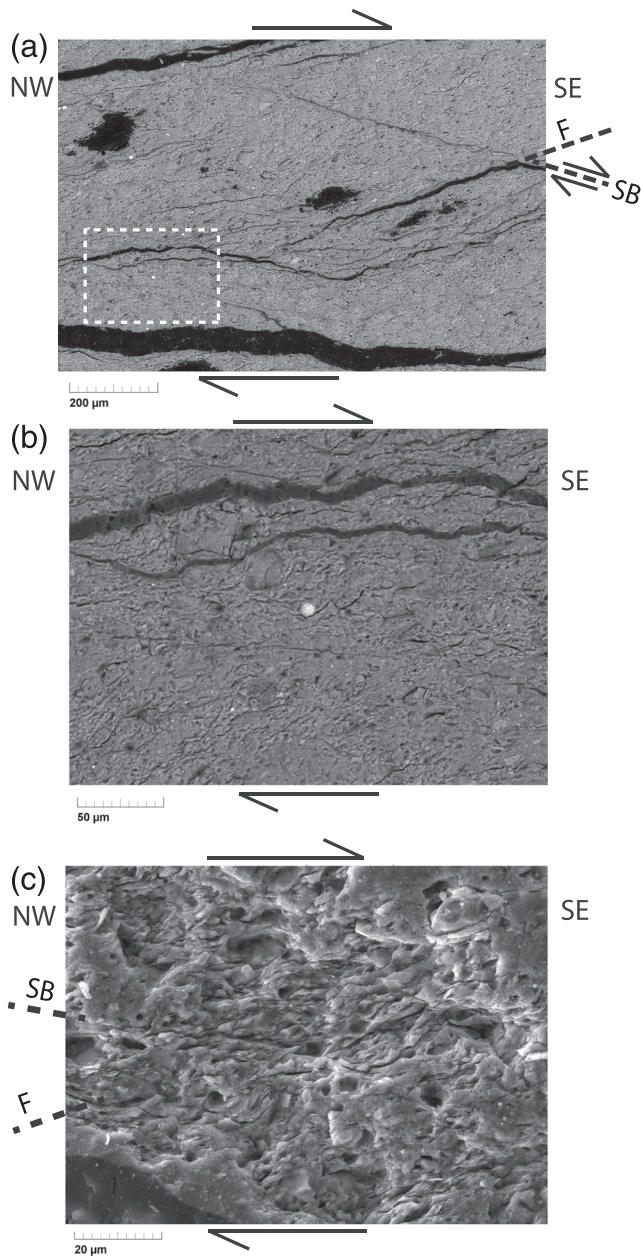


**Figure 15.** SEM images at various enlargements of the composite planar fabric in the main shear zone. (a) Typical composite planar fabric in the main shear zone showing foliation (F) deflected by shear band (SB). The deflection indicates a top-to-the-SE sense of shear. Location of image is given in Figure 12. Dashed white rectangle is the location of (b). (b) Detailed view of the planar composite fabric. (c) Detailed view of the planar composite fabric (location on Figure 12).

cuts poorly indurated sediments as well as clay-rich foliated gouges with a linear trace and with sharp boundaries. It is reminiscent of the principal slip zone (PSZ) of Sibson (2003) or the prominent fracture surface (PFS) of Chester and Chester (1998) and Chester et al. (2004). Whatever the terminology, these zones display the following characteristics: (1) compared to their lateral extension between several meters to several kilometers, they are very thin (1–100 mm). (2) The rock filling these zones is typically described as ultracataclasite, attesting of an extreme fragment size reduction. (3) Displacement remains localized along these zones. (4) Boundaries with surrounding fault rocks are sharp and planar or close to planar. These zones are interpreted as the site of propagation of seismic ruptures in the upper brittle crust, even if independent criteria such as the presence of pseudotachylyte are seldom observed (Chester & Chester, 1998). Since there is only one borehole, it is not possible to estimate the lateral extension of the through-going weakly foliated gouge interval of the C0004 shear zone. An area comparison between this interval and PSZs or PFSs is therefore not possible. However, the other characteristics (ultracomminution, sharp boundaries) suggest that this interval can be regarded as a PSZ (or PFS), along which seismic slip may have propagated, once or several times. Similarly, the remnant gouge observed (Figure 11a) can be interpreted as a former, possibly through-going, non-foliated gouge similar to that preserved along the through-going gouge interval. The injected gouges (Figure 11) observed in the upper northwestern corner of the C0004-13 thin section and above the lower subzone of the C0004 MSZ could be interpreted as granular injection veins as defined by Rowe et al. (2012) or by Smeraglia et al. (2016), possibly injected from the nearby through-going fault and associated weakly foliated gouge. Such an interpretation suggests that the injection was formed coseismically, as advocated by Lin (1996, 2011) or by Rowe et al. (2012). Lastly, the microbreccia outlining the fault bounding the MSZ of the C0007 intact core section suggests that some coseismic slip may have occurred along the basal décollement zone, subsequent to aseismic slip (creep) or slow slip events responsible for the formation of the foliated gouge.

The preservation of brittle and ductile deformation structures described here was also observed in cores retrieved during IODP drilling across the Papaku thrust, a major splay fault in the Hikurangi margin off New Zealand's North Island (Fagereng et al., 2019). Brittle structures include discrete faults and fractures and also breccias secant to bedding. Ductile structures include flow banding, i.e., layer-parallel, macroscopic flow typically mixing pure, and simple shear deformation.

#### 6.4. Fluid Flow Along the Studied Shear Zones

At the regional scale, both the splay fault zones and the décollement zones crossing the Nankai prism are considered as pathways for fluid flow (Kodaira et al., 2004; Park et al., 2002). In particular, based on tomographic imaging of the splay fault zone off Kii Peninsula, Kamei et al. (2012) interpreted the low-velocity zone encompassing the splay

fault zone as a fluid-rich zone. Surprisingly, microscopic evidence for fluid-rock interaction during or after deformation are scarce in thin sections from the C0004 and the C0007 shear zones. This evidence consists of (1) the presence of a redox front beneath the MSZ of the décollement fault for the C0007D intact core section and (2) the presence of (apparently) undeformed pyrite crystals along open fractures in the MSZ of the splay fault for the C0004D intact core section. Regarding observation (1), the simplest interpretation is that the redox front is the result of an oxidizing fluid flowing along or near the MSZ basal fault. Indeed, the

Hole number, type of fault and depth below seafloor	Name of zones or sub-zones	Type of fault rock	Internal planar structures	Style of deformation	Sense of displacement	
C0004D Splay fault (271.08-271.40 mbsf)	Upper secondary shear zone	Non-foliated gouge	None	brittle	undetermined	
	Upper secondary shear zone	Weakly foliated gouge	Incipient P foliation	ductile	top-to-the-SE	
	Upper sub-zone	Clayey matrix-rich foliated gouge (domain IA)	S/C-like structure	ductile	top-to-the-SE	
		Clast-rich foliated gouge (domain IB)	S/C-like structure	ductile	top-to-the-SE	
		Injected non-foliated gouge (granular injection vein)	None	brittle	undetermined	
	Main shear zone	Sharp and through-going gouge interval	Weakly-foliated gouge	Incipient P foliation	brittle	top-to-the-SE
		Lower sub-zone	Injected non-foliated gouge (granular injection vein)	None	brittle	undetermined
	Foliated gouge (domain IIA)		S/C-like structure	ductile	top-to-the-SE	
	Moderately foliated gouge (domain IIB)		S/C-like structure	ductile	top-to-the-SE	
	C0007D Basal décollement fault (438.28-438.64 mbsf)	Incipient shear zones	Foliated gouge	S/C-like structure	ductile	top-to-the-SE
Secondary shear zones		Foliated gouge	S/C-like structure	ductile	top-to-the-SE	
Main shear zone		Transition domain	S/C-like structure	ductile	top-to-the-SE	
		Foliated gouge	S/C-like structure	ductile	top-to-the-SE	
		Microbreccia formed at the expense of foliated gouge	None	brittle	undetermined	
		Fault surface (sharp and through-going)	N/A	brittle	undetermined	
Undeformed footwall		Redox front	N/A	N/A	N/A	

**Figure 16.** Summary of the various deformed zones and subzones and relevant microstructures observed in the two intact slabs from the splay fault and décollement fault. N/A: not applicable.

microbreccia outlining the basal fault shows a significant porosity (Figure 14) which could allow fluid circulation. Sea water trapped in accreted or subducted sediments could be a possible candidate for the oxidizing fluid. Indeed, during the evolution of accretionary prisms and more specifically during the various stages of the seismic cycle, pore water is expelled along the basal décollement fault (Fulton & Brodsky, 2016; Saffer & Tobin, 2011; Sibson, 2013). This upward flow of pore water could result in the development of a redox front. The presence of a redox front is reminiscent of observations reported by Yamaguchi, Cox, et al. (2011) in their study of a fossil megasplay fault in the Shimanto accretionary

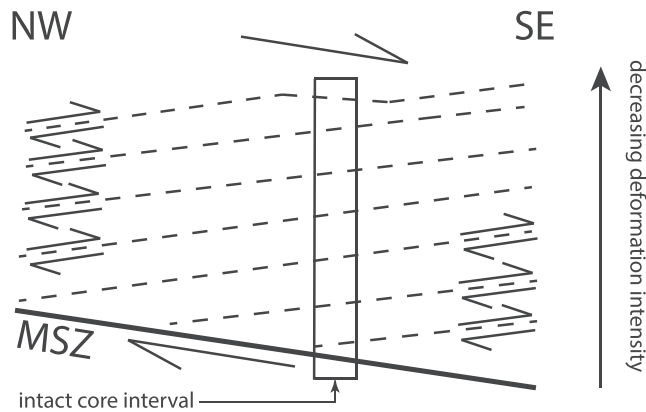


**Figure 17.** Sketch summarizing the main, secondary and incipient shear zone succession observed in the C0007 intact core interval (rectangle). Southeast-dipping shear zones are interpreted as undulating Y shears (Logan et al., 1992; Mandl et al., 1977; Swanson, 1988; Tchalenko, 1968) developed above the main shear zone (MSZ).

complex. Based on detailed chemical analyses of calcite veins, these authors suggest that during the prefailure stage of the megasplay fault, oxidizing fluids accumulate in the fault zone while during the immediately postfailure stage, reducing fluids transiently expelled from depth or generated in situ by coseismic mechanical or chemical reactions invade the fault zone. This repeating fault-valve behavior scenario is supposed to be in pace with the seismic cycle of the megasplay fault. Concerning the C0007D intact section, the observed redox front may not reflect a cyclic process but rather a single oxidizing fluid flow event. The presence of pyrite along open fractures in the upper and lower subzones of the MSZ of the C0004D intact interval may also reflect reducing fluid flow along the splay fault zone. The possible superposition of several oxidizing/reducing flow events along the two faults studied here, which could reflect a cyclic activity, should be investigated by detailed chemical analyses.

## 7. Conclusion

The recovery of intact core sections across two major faults in the Nankai accretionary prism along which stratigraphic inversions of ca. 2.09 myr (3.65-Ma sediments over 1.56-Ma sediments) for the splay fault branch and ca. 1.67 myr (5.32-Ma sediments over 3.65-Ma sediments) for the décollement fault are established allows one to draw important conclusions regarding the activity of these faults. (1) Deformation microstructures consist of microbreccia or weakly foliated gouge localized along fault slip surfaces and of foliated clayey gouges in shear zones of various importance (main, secondary, and ISZs). The splay fault at Hole C0004D is characterized by foliated gouge, by weakly foliated gouge and also by two granular injection veins possibly originating from the nearby weakly foliated gouge. The décollement fault at Hole C0007D is characterized by a foliated gouge and by a microbreccia along a fault truncating the foliated gouge. (2) For the two fault zones, fault activity is poly-phase. Regarding the upper subzone of the splay fault MSZ, formation of foliated gouge was followed by wear along a through-going slip surface and possibly coseismic gouge injection. Concerning the décollement fault, the formation of the MSZ foliated gouge was followed by propagation of the basal fault and formation of microbreccia at the expense of the overlying foliated gouge. (3) Evidence for oxidizing or reducing fluid flow along the décollement fault zone or along the splay fault is suggested by microscopic observations. (4) Along the splay fault core section, evidence for possible seismic slip is suggested by the presence of a weakly foliated gouge outlining a through-going well-localized slip zone and by the preservation of what is interpreted as granular injection veins derived from this weakly foliated gouge. Along the basal décollement fault zone core section, evidence for seismic slip is suggested by the preservation of microbreccia along a planar fault surface truncating preexisting foliated fault gouge.

## Acknowledgments

This research used samples and data provided by the International Ocean Drilling Program (IODP). The recovery of the two intact core sections was made possible thanks to the skillfulness of JAMSTEC and Marine Works Japan engineers and laboratory technicians onboard the R/V Chikyu. Polished thin sections described in this article are stored at the IODP Kochi Core Center. SEM images are stored at University of Franche-Comté DAT@OSU database (<https://dataosu.obs-besancon.fr>). We thank Kyuichi Kanagawa and two anonymous reviewers for their constructive comments.

## References

- Arai, R., Takahashi, T., Kodaira, S., Kaiho, Y., Nakanishi, A., Fujie, G., et al. (2016). Structure of the tsunamigenic plate boundary and low-frequency earthquakes in the southern Ryukyu Trench. *Nature Communications*, 7(1), 1–7. <https://doi.org/10.1038/ncomms12255>
- Araki, E., Saffer, D. M., Kopf, A. J., Wallace, L. M., Kimura, T., Machida, Y., et al., & IODP Expedition 365 shipboard scientists (2017). Recurring and triggered slow-slip events near the trench at the Nankai Trough subduction megathrust. *Science*, 356, 1157–1160.
- Baba, T., & Cummins, P. R. (2005). Contiguous rupture areas of two Nankai Trough earthquakes revealed by high-resolution tsunami waveform inversion. *Geophysical Research Letters*, 32, L08305. <https://doi.org/10.1029/2004GL022320>
- Baba, T., Cummins, P. R., Hori, T., & Kaneda, Y. (2006). High precision slip distribution of the 1944 Tonankai earthquake, inferred from tsunami waveforms: Possible slip on a splay fault. *Tectonophysics*, 426, 119–134. <https://doi.org/10.1016/j.tecto.2006.02.015>
- Chester, F. M., & Chester, J. S. (1998). Ultracataclastic structure and friction processes of the Punchbowl fault, San Andreas system, California. *Tectonophysics*, 295, 199–221.
- Chester, F. M., Chester, J. S., Kirschner, D. L., Schulz, S. E., & Evans, J. P. (2004). Structure of large displacement, strike-slip fault zones in the brittle continental crust. In G. D. Karner, B. Taylor, N. W. Driscoll, & D. L. Kohlstedt (Eds.), *Rheology and deformation in the lithosphere at continental margins*, (pp. 223–260). New York, NY: Columbia University Press.
- Chester, F. M., & Logan, J. M. (1987). Composite planar fabric of gouge from the Punchbowl fault, California. *Journal of Structural Geology*, 9(5/6), 621–634.
- Collot, J. Y., Agudelo, W., Ribodetti, A., & Marcaillou, B. (2008). Origin of a crustal splay fault and its relation to the seismogenic zone and underplating at the erosional north Ecuador-south Colombia oceanic margin. *Journal of Geophysical Research*, 113, B12102. <https://doi.org/10.1029/2008JB005691>
- Cowan, D. S. (1982). Origin of vein structure in slope sediments on the inner slope of the Middle America Trench off Guatemala. *Initial Reports of the Deep Sea Drilling Project*, 67, 645–650.

- DeDontney, N., & Rice, J. R. (2012). Tsunami wave analysis and possibility of splay fault rupture during the 2004 Indian Ocean earthquake. *Pure and Applied Geophysics*, 169(10), 1707–1735. <https://doi.org/10.1007/s00024-011-0438-4>
- Expedition 316 Scientists (2009a). Expedition 316 Site C0004. In M. Kinoshita et al., *Proceedings of the Integrated Ocean Drilling Program* (Vol. 314/315/316). <https://doi.org/10.2204/iodp.proc.314315316.133.2009>
- Expedition 316 Scientists (2009b). Expedition 316 Site C0007. In M. Kinoshita et al., *Proceedings of the Integrated Ocean Drilling Program* (Vol. 314/315/316) <https://doi.org/10.2204/iodp.proc.314315316.135.2009>
- Fagereng, Å., Savage, H. M., Morgan, J. K., Wang, M., Meneghini, F., Barnes, P. M., et al., & the IODP Expedition 372/375 Scientists (2019). Mixed deformation styles observed on a shallow subduction thrust, Hikurangi margin, New Zealand. *Geology*, 47(9), 872–876. <https://doi.org/10.1130/G46367.1>
- Faulkner, D. R., Mitchell, T. M., Behn, J., Hirose, T., & Shimamoto, T. (2011). Stuck in the mud? Earthquake nucleation and propagation through accretionary forearcs. *Geophysical Research Letters*, 38, L18303. <https://doi.org/10.1029/2011GL048552>
- Fisher, D., Mosher, D., Austin, J. A., Gulick, S. P., Masterlark, T., & Moran, K. (2007). Active deformation across the Sumatran forearc over the December 2004 Mw 9.2 rupture. *Geology*, 35(2), 99–102.
- Fukao, Y. (1979). Tsunami earthquakes and subduction processes near deep-sea trenches. *Journal of Geophysical Research*, 84(5), 2303–2314. <https://doi.org/10.1029/JB084iB05p02303>
- Fulton, P. M., & Brodsky, E. E. (2016). In situ observations of earthquake-driven fluid pulses within the Japan Trench plate boundary fault zone. *Geology*, 44(10), 851–854. <https://doi.org/10.1130/G38034.1>
- Gulick, S. P., Austin, J. R., McNeill, L. C., Bangs, N. L., Martin, K. M., Henstock, T. J., et al. (2011). Updip rupture of the 2004 Sumatra earthquake extended by thick indurated sediments. *Nature Geoscience*, 4(7), 453–456. <https://doi.org/10.1038/NGEO1176>
- Hamada, Y., Sakaguchi, A., Tanikawa, W., Yamaguchi, A., Kameda, J., & Kimura, G. (2015). Estimation of slip rate and fault displacement during shallow earthquake rupture in the Nankai subduction zone. *Earth, Planets and Space*, 67(1), 1–12. <https://doi.org/10.1186/s40623-015-0208-0>
- Heki, K. (2007). Secular, transient and seasonal crustal movements in Japan from a dense GPS array: Implication for plate dynamics in convergent boundaries. In T. Dixon, & C. Moore (Eds.), *The seismogenic zone of subduction thrust faults*, (pp. 512–539). New York, NY: Columbia University Press.
- Hirono, T., Ishikawa, T., Matsumoto, H., Hamed, J., Yabuta, H., & Mukoyoshi, H. (2014). Re-evaluation of frictional heat recorded in the dark gouge of the shallow part of a megasplay fault at the Nankai trough. *Tectonophysics*, 626, 157–169. <https://doi.org/10.1016/j.tecto.2014.04.020>
- Hirono, T., Ujiie, K., Ishikawa, T., Mishima, T., Hamada, Y., Tanimizu, M., et al. (2009). Estimation of temperature rise in a shallow slip zone of the megasplay fault in the Nankai Trough. *Tectonophysics*, 478, 215–220. <https://doi.org/10.1016/j.tecto.2009.08.001>
- Hsu, S. K., Yeh, Y. C., Sibuet, J. C., Doo, W. B., & Tsai, C. H. (2013). A mega-splay fault system and tsunami hazard in the southern Ryukyu subduction zone. *Earth and Planetary Science Letters*, 362, 99–107. <https://doi.org/10.1016/j.epsl.2012.11.053>
- Ichinose, G. A., Thio, H. K., Somerville, P. G., Sato, T., & Ishii, T. (2003). Rupture process of the 1944 Tonankai earthquake (Ms 8.1) from the inversion of teleseismic and regional seismograms. *Journal of Geophysical Research*, 108(10), 2497. <https://doi.org/10.1029/2003JB002393>
- Ikari, M. J., & Saffer, D. M. (2011). Comparison of frictional strength and velocity dependence between fault zones in the Nankai accretionary complex. *Geochemistry, Geophysics, Geosystems*, 12, Q0AD11. <https://doi.org/10.1029/2010GC003442>
- Ikari, M. J., Saffer, D. M., & Marone, C. (2009). Frictional and hydrologic properties of a major splay fault system, Nankai subduction zone. *Geophysical Research Letters*, 36, L20313. <https://doi.org/10.1029/2009GL040009>
- Ito, Y., & Obara, K. (2006). Dynamic deformation of the accretionary prism excites very low frequency earthquakes. *Geophysical Research Letters*, 33, L02311. <https://doi.org/10.1029/2005GL025270>
- Kamei, R., Pratt, R. G., & Tsuji, T. (2012). Waveform tomography imaging of a megasplay fault system in the seismogenic Nankai subduction zone. *Earth and Planetary Science Letters*, 317–318, 343–353. <https://doi.org/10.1016/j.epsl.2011.10.042>
- Kikuchi, M., Nakamura, M., & Yoshikawa, K. (2003). Source rupture processes of the 1944 Tonankai Earthquake and the 1945 Mikawa Earthquake derived from low-gain seismograms. *Earth, Planets and Space*, 55, 159–172.
- Kimura, G., Sreaton, E. J., & Curewitz, D. (2007). Integrated Ocean Drilling Program Expedition 316 Scientific Prospectus NanTroSEIZE Stage 1: NanTroSEIZE shallow megasplay and frontal thrusts. <https://doi.org/10.2204/iodp.sp.316>
- Kimura, G., Sreaton, E. J., Curewitz, D., & the Expedition 316 Scientists (2008). Nan-TroSEIZE Stage 1A: Nan-TroSEIZE shallow megasplay and frontal thrusts. *Integrated Ocean Drilling Program Preliminary Report*, 316. <https://doi.org/10.2204/iodp.pr.316>
- Kinoshita, M., Tobin, H., Ashi, J., Kimura, G., Lallemand, S., Sreaton, E. J., et al., & the Expedition 314/315/316 Scientists (2009). *Proceedings of the Integrated Ocean Drilling Program, Volume 314/315/316*: Washington, D. C., Integrated Ocean Drilling Program Management International, Inc. <https://doi.org/10.2204/iodp.proc.314315316.133.2009>
- Kodaira, S., Iidaka, T., Kato, A., Park, J. O., Iwasaki, T., & Kaneda, Y. (2004). High pore fluid pressure may cause silent slip in the Nankai Trough. *Science*, 304, 1295–1298.
- Kondo, H., Kimura, G., Masago, H., Ohmori-Ikehara, K., Kitamura, Y., Ikesawa, E., et al. (2005). Deformation and fluid flow of a major out-of-sequence thrust located at seismogenic depth in an accretionary complex: Nobeoka Thrust in the Shimanto Belt, Kyushu, Japan. *Tectonics*, 24, TC6008. <https://doi.org/10.1029/2004TC001655>
- Lin, A. (1996). Injection veins of crushing-originated pseudotachylyte and fault gouge formed during seismic faulting. *Engineering Geology*, 43, 213–224.
- Lin, A. (2011). Seismic slip recorded by fluidized ultracataclastic veins formed in a coseismic shear zone during the 2008 Mw 7.9 Wenchuan earthquake. *Geology*, 39(6), 547–550. <https://doi.org/10.1130/G32065.1>
- Logan, J. M., Dengo, C. A., Higgs, N. G., & Wang, Z. Z. (1992). Fabrics of experimental fault zones: Their development and relationship to mechanical behavior. In B. Evans, & T.-f. Wong (Eds.), *Fault mechanics and transport properties of rocks*, (pp. 33–67). London: Academic Press.
- Mandl, G., De Jong, L. N. J., & Maltha, A. (1977). Shear zones in granular material. *Rock Mechanics*, 9, 95–144.
- Melnick, D., Moreno, M., Motagh, M., Cisternas, M., & Wesson, R. L. (2012). Splay fault slip during the Mw 8.8 2010 Maule Chile earthquake. *Geology*, 40(3), 251–254. <https://doi.org/10.1130/G32712.1>
- Miller, M. G. (1996). Ductility in fault gouge from a normal fault system, Death Valley, California: A mechanism for fault-zone strengthening and relevance to paleoseismicity. *Geology*, 24(7), 603–606.
- Moore, G. F., Bangs, N. L., Taira, A., Kuramoto, S., Pangborn, E., & Tobin, H. J. (2007). Three dimensional splay fault geometry and implications for tsunami generation. *Science*, 318(5853), 1128–1131. <https://doi.org/10.1126/science.1147195>

- Moore, G.F., Park, J.O., Bangs, N.L., Gulick, S.P., Tobin, H.J., Nakamura, Y., et al. (2009). Structural and seismic stratigraphic framework of the NanTroSEIZE Stage 1 transect. In M. Kinoshita et al., *Proceedings of the Integrated Ocean Drilling Program* (Vol. 314/315/316). <https://doi.org/10.2204/iodp.proc.314315316.314315102.314312009>
- Moore, J. C., Diebold, J., Fisher, M. A., Sample, J., Brocher, T., Talwani, M., et al. (1991). EDGE deep seismic reflection transect of the Eastern Aleutian Arc-Trench layered lower crust reveals underplating and continental growth. *Geology*, *19*(5), 420–424. <https://doi.org/10.1130/0091-7613>
- Nakanishi, A., Kodaira, S., Miura, S., Ito, A., Sato, T., Park, J. O., et al. (2008). Detailed structural image around splay-fault branching in the Nankai subduction seismogenic zone: Results from a high-density ocean bottom seismic survey. *Journal of Geophysical Research*, *113*, B03105. <https://doi.org/10.1029/2007JB004974>
- Obana, K., & Kodaira, S. (2009). Low-frequency tremors associated with reverse faults in a shallow accretionary prism. *Earth and Planetary Science Letters*, *287*, 168–174. <https://doi.org/10.1016/j.epsl.2009.08.005>
- Park, J. O., Fujie, G., Wijerathne, L., Hori, T., Kodaira, S., Fukao, Y., et al. (2010). A low-velocity zone with weak reflectivity along the Nankai subduction zone. *Geology*, *38*(3), 283–286. <https://doi.org/10.1130/G30205.1>
- Park, J. O., & Kodaira, S. (2012). Seismic reflection and bathymetric evidences for the Nankai earthquake rupture across a stable segment-boundary. *Earth, Planets and Space*, *64*, 299–303. <https://doi.org/10.5047/eps.2011.10.006>
- Park, J. O., Tsuru, T., Kodaira, S., Cummins, P. R., & Kaneda, Y. (2002). Splay fault branching along the Nankai subduction zone. *Science*, *297*(5584), 1157–1160. <https://doi.org/10.1126/science.1074111>
- Park, J. O., Tsuru, T., Kodaira, S., Nakanishi, A., Miura, S., Kaneda, Y., & Kono, Y. (2000). Out-of-sequence thrust faults developed in the coseismic slip zone of the 1946 Nankai earthquake (Mw = 8.2) off Shikoku, southwest Japan. *Geophysical Research Letters*, *27*(7), 1033–1036.
- Passchier, C. W., & Trouw, R. A. (2005). *Microtectonics* (2nd ed., p. 372). Berlin: Springer.
- Reinen, L. A. (2000). Seismic and aseismic slip indicators in serpentinite gouge. *Geology*, *28*(2), 135–138.
- Rowe, C. D., Kirkpatrick, J. D., & Brodsky, E. E. (2012). Fault rock injections record paleo-earthquakes. *Earth and Planetary Science Letters*, *335*, 154–166. <https://doi.org/10.1016/j.epsl.2012.04.015>
- Rutter, E. H., Maddock, R. H., Hall, S. H., & White, S. H. (1986). Comparative microstructures of natural and experimentally produced clay-bearing fault gouges. *Pure and Applied Geophysics*, *124*(1/2), 3–30.
- Saffer, D. M., & Tobin, H. J. (2011). Hydrogeology and mechanics of subduction zone forearcs: Fluid flow and pore pressure. *Annual Reviews of Earth and Planetary Sciences*, *39*, 157–186. <https://doi.org/10.1146/annurev-earth-040610-133408>
- Saito, T., Ujiie, K., Tsutsumi, A., Kameda, J., & Shibazaki, B. (2013). Geological and frictional aspects of very-low frequency earthquakes in an accretionary prism. *Geophysical Research Letters*, *40*, 703–708. <https://doi.org/10.1002/grl.50175>
- Sakaguchi, A., Chester, F., Curewitz, D., Fabbri, O., Goldsby, D., Kimura, G., et al. (2011). Seismic slip propagation to the up-dip end of plate boundary subduction interface faults: Vitritinite reflectance geothermometry on Integrated Ocean Drilling Program NanTro SEIZE cores. *Geology*, *39*(4), 395–398. <https://doi.org/10.1130/G31642.1>
- Satake, K. (1993). Depth distribution of coseismic slip along the Nankai Trough, Japan, from joint inversion of geodetic and tsunami data. *Journal of Geophysical Research*, *98*(B3), 4553–4565.
- Scholz, C. H. (2002). *The mechanics of earthquakes and faulting* (2nd ed., p. 471). New York, NY: Cambridge University Press.
- Screaton, E.J., Kimura, G., Curewitz, D. and the Expedition 316 Scientists (2009). Expedition 316 summary. In M. Kinoshita et al., *Proceedings of the Integrated Ocean Drilling Program* (Vol. 314/315/316). <https://doi.org/10.2204/iodp.proc.314315316.131.2009>
- Seno, T., Stein, S., & Gripp, A. E. (1993). A model for the motion of the Philippine Sea plate consistent with NUVEL-1 and geological data. *Journal of Geophysical Research*, *98*, 17,941–17,948. <https://doi.org/10.1029/93JB00782>
- Sibson, R. H. (1977). Fault rocks and fault mechanisms. *Journal of the Geological Society*, *133*, 191–213.
- Sibson, R. H. (2003). Thickness of the seismic slip zone. *Bulletin of the Seismological Society of America*, *93*(3), 1169–1178.
- Sibson, R. H. (2013). Stress switching in subduction forearcs: Implications for overpressure containment and strength cycling on mega-thrusts. *Tectonophysics*, *600*, 142–152. <https://doi.org/10.1016/j.tecto.2013.02.035>
- Smeraglia, L., Aldega, L., Billi, A., Carminati, E., & Doglioni, C. (2016). Phyllosilicate injection along extensional carbonate-hosted faults and implications for co-seismic slip propagation: Case studies from the central Apennines, Italy. *Journal of Structural Geology*, *93*, 29–50. <https://doi.org/10.1016/j.jsg.2016.10.003>
- Sugioka, H., Okamoto, T., Nakamura, T., Ishihara, Y., Ito, A., Obana, K., et al. (2012). Tsunamigenic potential of the shallow subduction plate boundary inferred from slow seismic slip. *Nature Geoscience*, *5*, 414–418. <https://doi.org/10.1038/NCEO1466>
- Swanson, M. T. (1988). Pseudotachylite-bearing strike-slip duplex structures in the Fort Foster Brittle Zone, S. Maine. *Journal of Structural Geology*, *10*(8), 813–828.
- Tanioka, Y., & Satake, K. (2001). Detailed coseismic slip distribution of the 1944 Tonankai Earthquake estimated from tsunami waveforms. *Geophysical Research Letters*, *28*(6), 1075–1078. <https://doi.org/10.1029/2000GL012284>
- Tchalenko, J. S. (1968). The evolution of kink-bands and the development of compression textures in sheared clays. *Tectonophysics*, *6*(2), 159–174.
- Tobin, H., Kinoshita, M., Ashi, J., Lallemand, S., Kimura, G., Screaton, E., et al., and the Expedition 314/315/316 Scientists (2009). NanTroSEIZE stage 1 expeditions: Introduction and synthesis of key results. In M. Kinoshita et al., *Proceedings of the Integrated Ocean Drilling Program* (Vol. 314/315/316). <https://doi.org/10.2204/iodp.proc.314315316.101.2009>
- Tobin, H. J., & Kinoshita, M. (2006). NanTroSEIZE: The IODP Nankai Trough seismogenic experiment. *Scientific Drilling*, *2*, 23–27. <https://doi.org/10.2204/iodp.sd.2.06.2006>
- Tsuji, T., Kimura, G., Okamoto, S., Kono, F., Mochinaga, H., Saeki, T., & Tokuyama, H. (2006). Modern and ancient seismogenic out-of-sequence thrusts in the Nankai accretionary prism: Comparison of laboratory-derived physical properties and seismic reflection data. *Geophysical Research Letters*, *33*, L18309. <https://doi.org/10.1029/2006GL027025>
- Tsutsumi, A., Fabbri, O., Karpoff, A. M., Ujiie, K., & Tsujimoto, A. (2011). Friction velocity dependence of clay-rich fault material along a megasplay fault in the Nankai subduction zone at intermediate to high velocities. *Geophysical Research Letters*, *38*, L19301. <https://doi.org/10.1029/2011GL049314>
- Ujiie, K., & Kimura, G. (2014). Earthquake faulting in subduction zones: Insights from fault rocks in accretionary prisms. *Progress in Earth and Planetary Science*, *1*(1), 1–30. <https://doi.org/10.1186/2197-4284-1-7>
- Ujiie, K., & Tsutsumi, A. (2010). High-velocity frictional properties of clay-rich fault gouge in a megasplay fault zone, Nankai subduction zone. *Geophysical Research Letters*, *37*, L24310. <https://doi.org/10.1029/2010GL046002>
- Waldhauser, F., Schaff, D. P., Diehl, T., & Engdahl, R. (2012). Splay faults imaged by fluid-driven aftershocks of the 2004 Mw 9.2 Sumatra-Andaman earthquake. *Geology*, *40*(3), 243–246. <https://doi.org/10.1130/G32420.1>

- Yamaguchi, A., Cox, S. F., Kimura, G., & Okamoto, S. (2011). Dynamic changes in fluid redox state associated with episodic fault rupture along a megasplay fault in a subduction zone. *Earth and Planetary Science Letters*, *302*, 369–377. <https://doi.org/10.1016/j.epsl.2010.12.029>
- Yamaguchi, A., Sakaguchi, A., Sakamoto, T., Iijima, K., Kameda, J., Kimura, G., et al. (2011). Progressive illitization in fault gouge caused by seismic slip propagation along a megasplay fault in the Nankai Trough. *Geology*, *39*(11), 995–998. <https://doi.org/10.1130/G32038.1>